The Distribution of Atomic Hydrogen in the Host Galaxies of FRBs

This peer-reviewed article has been accepted for publication in Publications of the Astronomical Society of Australia but not yet copyedited or typeset, and so may be subject to change during the production process.

The article is considered published and may be cited using its DOI. 10.1017/pasa.2025.10123

The Distribution of Atomic Hydrogen in the Host Galaxies of FRBs

H. Roxburgh,[1] M. Glowacki,[1,2,3] A. Bera,[1] C. W. James,[1] N. Deg,[4] Q. Huang,[5] K. Lee-Waddell,[6,7,1] J. Wang,[5] M. Caleb,[8] A. T. Deller,[9] L. N. Driessen,[8] A. C. Gordon,[10] K. M. Hess,[11,12] J. X. Prochaska,[13,14,15] R. M. Shannon,[9] Y. Wang,[9] Z. Wang,[1] and D. Yang[5]

[1]International Centre for Radio Astronomy Research, Curtin University, Bentley, WA 6102, Australia
[2]Institute for Astronomy, University of Edinburgh, Royal Observatory, Edinburgh, EH9 3HJ, United Kingdom
[3]Inter-University Institute for Data Intensive Astronomy, Department of Astronomy, University of Cape Town, Cape Town, South Africa
[4]Department of Physics, Engineering Physics, and Astronomy,Queen's University, Kingston ON K7L 3N6, Canada
[5]Kavli Institute for Astronomy and Astrophysics, Peking University, Beijing 100871, China; Department of Astronomy, School of Physics, Peking University, Beijing 100871, China
[6]Australian SKA Regional Centre (AusSRC) - The University of Western Australia, 35 Stirling Highway, Crawley WA 6009, Australia
[7]CSIRO Space and Astronomy, PO Box 1130, Bentley WA 6102, Australia
[8]Sydney Institute for Astronomy, School of Physics, The University of Sydney, NSW 2006, Australia
[9]Centre for Astrophysics and Supercomputing, Swinburne University of Technology, Hawthorn, VIC, 3122, Australia
[10]Center for Interdisciplinary Exploration and Research in Astrophysics (CIERA) and Department of Physics and Astronomy, Northwestern University, Evanston, IL 60208, USA
[11]Department of Space, Earth and Environment, Chalmers University of Technology, Onsala Space Observatory, SE-43992 Onsala, Sweden
[12]ASTRON, The Netherlands Institute for Radio Astronomy, Postbus 2, 7990 AA, Dwingeloo, The Netherlands
[13]Department of Astronomy and Astrophysics, University of California, Santa Cruz, CA 95064, USA
[14]Kavli Institute for the Physics and Mathematics of the Universe (Kavli IPMU), 5-1-5 Kashiwanoha, Kashiwa, 277-8583, Japan
[15]Division of Science, National Astronomical Observatory of Japan, 2-21-1 Osawa, Mitaka, Tokyo, 181-8588, Japan
Author for correspondence: H. Roxburgh, Email: hugh.roxburgh@postgrad.curtin.edu.au.

Abstract

We probe the atomic hydrogen (HI) emission from the host galaxies of fast radio bursts (FRBs) to investigate the emerging trend of disturbance and asymmetry in the population. Quadrupling the sample size, we detect 16 out of 17 new hosts in HI, with the single non-detection arising in a galaxy known to be transitioning towards quiescence. With respect to typical local Universe galaxies, FRB hosts are generally massive in HI ($M_{\rm HI} > 10^9\ M_\odot$), which aligns with previous studies reporting that FRB hosts also tend to have high stellar masses and are star-forming. However, they span a broad range of other HI derived properties. Using visual inspection alongside various asymmetry metrics, we identify six unambiguously settled host galaxies, demonstrating for the first time that a disturbed HI morphology is not a universal feature of FRB host galaxies. However, we find another six that show clear signs of disturbance, one borderline case, and three which require deeper or more targeted observations to reach a conclusion; this brings the confirmed ratio of disturbed-to-settled FRB hosts to 11:6. Given that roughly a 1:1 ratio is expected for random background galaxies of similar type, our observed ratio yields a p-value of 0.222. Therefore, we conclude that contrary to earlier indications, there is no statistically significant excess of HI disturbance in this sample of FRB host galaxies with respect to the general galaxy population, and hence we find no evidence for a fundamental connection between FRB progenitor formation and merger-induced star formation activity.

1. Introduction

Fast radio bursts (FRBs) are energetic pulses of radio emission that generally last for a few milliseconds in timescale (Lorimer et al. 2007). Whilst their extragalactic origins are well established (Chatterjee et al. 2017; Bannister et al. 2019), their generation mechanisms remain unclear, despite significant advances in the field. Dozens of progenitor models have been proposed to explain the phenomena, from outbursting neutron stars to interacting black holes (for reviews, see Platts et al. 2019; Petroff, Hessels, and Lorimer 2019). The former, specifically young, highly magnetised neutron stars or magnetars, are favoured within the community due to observations of energetic FRBs found to be embedded within persistent radio sources (PRSs) (e.g. Metzger, Berger, and Margalit 2017). This link was strengthened in 2020 with the detection of an FRB from a magnetar within our galaxy (CHIME/FRB Collaboration et al. 2020; Bochenek et al. 2020), although its isotropic-equivalent energy falls nearly 30 times lower than the next weakest FRB.

Since their discovery, the population of detected FRBs has rapidly expanded, primarily due to dedicated observations from the Australian Square Kilometre Array Pathfinder (ASKAP; Hotan et al. 2021; Bannister et al. 2019; Shannon et al. 2024), the Canadian Hydrogen Intensity Mapping Experiment (CHIME; Bandura et al. 2014; CHIME/FRB Collaboration et al. 2021), MeerKAT (Jonas and The MeerKAT Team 2016; Bezuidenhout et al. 2022), and the Deep Synoptic Array (DSA; Kocz et al. 2019; Ravi et al. 2023; Connor et al. 2025). Crucially, improvements to spatial resolution have allowed many FRBs to be localised to arcsecond or better accuracy, allowing for deep follow up photometry and spectroscopy of their host galaxies and environments (e.g. Bannister et al. 2019; Heintz et al. 2020; Mannings et al. 2021; Bhandari et al. 2022; Gordon et al. 2023; Ryder et al. 2023; Sharma et al. 2024; CHIME/FRB Collaboration et al. 2025). Such localisations are key to revealing the environments of FRBs and unlocking

https://doi.org/10.1017/pasa.2025.10123 Published online by Cambridge University Press

their potential for cosmological studies (e.g. McQuinn 2014; Macquart et al. 2020; James et al. 2022; Connor et al. 2025).

As of September 2025, over 100 host galaxies have been identified, spanning redshifts out to z =2.15. These galaxies tend to be star-forming spiral galaxies, though most other galactic parameters such as stellar mass and mass-weighted age are highly varied (Bhandari et al. 2022; Gordon et al. 2023). These observations broadly support a magnetar progenitor hypothesis, as magnetars are expected to trace star formation through a core-collapse supernovae generation channel (Metzger, Berger, and Margalit 2017). However, a number of counterexamples, such as a localisation to a globular cluster (Kirsten et al. 2022), and several to quiescent galaxies (Eftekhari et al. 2025; Shah et al. 2025), muddy the waters. Furthermore, no statistically significant trend differing the hosts of repeating and apparently non-repeating FRBs has been observed (Gordon et al. 2023; Sharma et al. 2024), despite significant evidence suggesting fundamental differences in their respective origins (CHIME/FRB Collaboration et al. 2021).

Beyond analysis of the optical output of these host galaxies, a number of studies have been conducted on their atomic hydrogen (HI) gas emission (Michalowski 2021; Kaur, Kanekar, and Prochaska 2022; Glowacki et al. 2023; Lee-Waddell et al. 2023; Glowacki et al. 2024). At redshifts greater than 0.1, the HI line becomes weak and contaminated by RFI; with much of the localised FRB population lying beyond this redshift, only six host galaxies (excluding the Milky Way) have thus far been probed. All six of these galaxies have been detected in HI, an expected result considering the star-forming nature of most hosts as derived from optical observations. Interestingly, a trend has emerged, with five of six of these detections exhibiting either a strongly asymmetric HI spectrum or a highly disturbed spatial gas distribution. The single apparently symmetric profile, that of FRB 20211127I, was analysed with a low resolution and low signal-to-noise ratio (SNR) ASKAP observation, and thus its lack of disturbance was considered inconclusive (Glowacki et al. 2023).

Such features, which are well documented in the literature (e.g. Holwerda et al. 2011; Espada et al. 2011; Bok et al. 2019; Reynolds, Westmeier, and Staveley-Smith 2020), are attributed to recent or ongoing disruptions to the galactic environment. The gaseous disk is sensitive to both external and internal perturbative mechanisms, including tidal interactions and mergers, ram pressure stripping, and feedback from supernovae or active galactic nuclei (AGN; Yu et al. 2022). Disturbed HI distributions are not uncommon; many studies have found that a significant fraction of galaxies exhibit some sign of disturbance. Historical studies using single dish instruments focused on the asymmetry of the 1D profile; early estimates found that at least 50% of galaxies exhibit spectra with some level of asymmetry (Richter and Sancisi 1994; Haynes et al. 1998; Matthews, Driel, and Gallagher III 1998). However, more recent studies use more stringent cutoffs; including these results (Espada et al. 2011; Watts et al. 2020; Reynolds, Westmeier, and Staveley-Smith 2020; Yu et al. 2022) and reevaluating the historical ones find anywhere between 10-40% of galaxies exhibit asymmetric HI line profiles.

In comparison, few studies have investigated similar properties in the spatial distribution of resolved HI galaxies (Holwerda et al. 2011; van Eymeren et al. 2011). Reynolds et al. (2020) recently probed ∼120 galaxies from the LVHIS (Barbel S. Koribalski et al. 2018), VIVA (Chung et al. 2009), and HALOGAS (Heald et al. 2011) surveys, finding similar rates of asymmetry. However, with a number of more advanced interferometric observatories currently in the process of conducting large HI surveys of resolved galaxies — such as the Widefield ASKAP L-band Legacy All-sky Blind surveY (WALLABY, Bärbel S. Koribalski et al. 2020) on ASKAP, the HI project within the MeerKAT International GigaHertz Tiered Extragalactic Exploration survey (MIGHTEE-HI, Maddox et al. 2021), and the Apertif HI surveys (Adams et al. 2022) on the Westerbork Synthesis Radio Telescope (WRST, van Cappellen et al. 2022) — many more observations will be made to properly pin down morphological asymmetry in HI disks.

Overall, the exact fraction of disturbed galaxies measured by each study is highly dependent on the samples used (e.g., isolated vs galaxy pairs), the observational properties (e.g. resolution and sensitivity), the method of quantification, and the point of cutoff in these methods above which a profile is considered disrupted. However, it can generally be said that disturbances are common, and are likely present in up to half of the galaxy population.

Thus, given the low number of hosts probed, the early trend towards asymmetry in the population — with a ratio of 5:0 or 5:1 — is not necessarily significant at this stage. However, if this trend perseveres as more host galaxies are observed in HI, it may indicate a connection between FRBs and a recent enhancement of star formation due to galactic interaction (Michalowski 2021). Indeed, studies over the past few decades have identified higher star formation rates in merging galaxies (e.g. Alonso et al. 2004; Darg et al. 2010). Such a scenario would lend further credence to so called 'fast track' FRB progenitors such as magnetars, which are expected to trace star formation.

To this end, we set forth to expand the sample size of FRB host galaxies observed in HI, and search for signs of asymmetry in their spectral and spatial profiles. This paper is structured as follows: in Section 2, we outline the sample of FRB host galaxy targets, and detail the observations and processing methods used to acquire HI information. In Section 3, we present our detections and the HI properties of the sample. Section 4 highlights the various methods we use to assess the disturbance/asymmetry of a detection. We evaluate each target in Section 5, and discuss the implications of these findings in Section 6. Finally, we summarise and conclude in Section 7.

2. Data

2.1 FRB Host Galaxy Targets

The FRBs selected for this study are taken from published datasets from the CRAFT survey (Commensal Real-time ASKAP Fast Transients; J. P. Macquart et al. 2010; Bannister et al. 2019; Shannon et al. 2024), the CHIME/FRB Collaboration (CHIME/FRB Collaboration et al. 2021; CHIME/FRB Collaboration et al. 2025),

https://doi.org/10.1017/pasa.2025.10123 Published online by Cambridge University Press

Table 1. FRB host galaxies analysed in this study. Repeaters are shown with a dagger.

FRB Name	Dataset	Host Galaxy	R.A. (°)	Dec. (°)	Redshift	Reference
FRB 20181220A	CHIME	2MFGC 17440	348.6982	48.3421	0.02746	Bhardwaj et al. (2024)
FRB 20181223C	CHIME	SDSS J120340.98+273251.4	180.9207	27.5476	0.03024	Bhardwaj et al. (2024)
FRB 20190418A	CHIME	SDSS J042314.96+160425.6	65.8123	16.0738	0.07132	Bhardwaj et al. (2024)
FRB 20190425A	CHIME	UGC 10667	255.6625	21.5767	0.03122	Bhardwaj et al. (2024)
FRB 20200223B†	CHIME	SDSS J003304.68+284952.6	8.2695	28.8313	0.06024	Ibik et al. (2023)
FRB 20200723B	CHIME	NGC 4602	190.1538	-5.1328	0.0085	Shin et al. (2024)
FRB 20201123A	MeerTRAP	J173438.35-504550.4	263.6596	-50.7641	0.0507	Rajwade et al. (2022)
FRB 20210405I	MeerTRAP	2MASS J1701249-4932475	255.3537	-49.5465	0.0656	Driessen et al. (2024b)
FRB 20211127I	CRAFT	WALLABY J131913−185018	199.8082	-18.8378	0.04695	Glowacki et al. (2023)
FRB 20211212A	CRAFT	SDSS J102924.22+012139.2	157.3509	1.3608	0.0715	Shannon et al. (2024)
FRB 20231229A	CHIME	UGC 1234	26.4658	35.1110	0.0190	CHIME/FRB Collaboration et al. (2025)
FRB 20231230A	CHIME	J045109.39+022205.02	72.7887	2.3681	0.0298	CHIME/FRB Collaboration et al. (2025)
FRB 20240201A	CRAFT	WISEA J095937.44+140519.4	149.9060	14.0887	0.04273	Shannon et al. (2024)
FRB 20240210A	CRAFT	WISEA J003506.47−281619.1	8.7768	-28.2723	0.02369	Shannon et al. (2024)
FRB 20240312D	CRAFT	WISEA J032629.50-543557.2	51.6227	-54.5993	0.04973	Gordon et al. (2025)
FRB 20240615B	CRAFT	WISEA J021551.26-143729.8	33.9633	-14.6247	0.0730	Gordon et al. (2025)
FRB 20250316A	CHIME	NGC 4141	182.4472	58.8492	0.00635	CHIME/FRB Collaboration et al. (2025)

and the MeerTRAP survey (More TRAnsients and Pulsars; Bezuidenhout et al. 2022; Rajwade et al. 2022; Driessen et al. 2024a).

We place two criteria on targets for inclusion in this study. The first is that the host association is robust, which is evaluated through the PATH framework (Probabilistic Association of Transients to their Hosts; Aggarwal et al. 2021). PATH employs a Bayesian approach to calculate the probability a given transient event is associated with a galaxy, based on the event's localisation and the galaxy's magnitude and size. Following the convention used in Bhandari et al. (2022) and Gordon et al. (2023), we consider PATH posterior probabilities P(O|x) ≥ 0.9 to be robust host associations.

Our second criterion is that the redshifts of the target host galaxies are ≤ 0.1. This is due to both the weak intensity of the HI line, and also the prevalence of contaminating radio frequency interference (RFI) below 1300 MHz ($z \sim 0.092$), largely due to the Global Navigation Satellite System (GNSS).

Based on these cuts, our sample consists of nine CHIME FRBs, six CRAFT FRBs, and two MeerTRAP FRBs. All but one CHIME target (FRB 20200223B) are apparently non-repeating bursts ("non-repeaters" herein), and one of the CRAFT targets (FRB 20211127I) is the FRB previously analysed in Glowacki et al. (2023). The details of their host galaxies are presented in Table 1.

2.2 HI Observations & Processing

We first searched for archival HI datasets, and found observations of the hosts of FRB 20231229A and FRB 20250316A (CHIME/FRB Collaboration et al. 2025). Both galaxies have been observed in HI twice; we take the most recent spectra available in each case, corresponding to an ALFALFA (Arecibo Legacy Fast ALFA; Haynes et al. 2018) survey observation and an Effelsberg 100-m observation (Haynes et al. 1999) respectively. Both of these are at spectral resolutions of 11 km s^{-1}, with single-dish beams encompassing several times the angular size of the galaxy.

A search of the MeerKAT archive hosted by the South African Radio Astronomical Observatory (SARAO) revealed that the coordinates of three targets were contained in archival L band observations. The host of FRB 20200723B (Shin et al. 2024) was the target of a 0.5 hour 4K channelisation (corresponding to $\sim$44 km s^{-1} resolution) pointing from "Part 2: 1.28 GHz MeerKAT survey of 12MGS Galaxies in the Southern Hemisphere", project ID SCI-20220822-LM-01, capture block ID 1671245181. The host of FRB 20201123A (Rajwade et al. 2022) was contained in a 1 hour 4K channelisation pointing by the "Legacy Survey of the Galactic Plane", project ID SSV-20180505-FC-01, capture block ID 1610418665, a distance of 0.4° from the phase centre. The host of FRB 20231230A (CHIME/FRB Collaboration et al. 2025) was contained in a 7.5 hour 4K channelisation pointing from the proposal "Observation of the galaxy cluster A520", project ID SCI-20210212-SG-01, capture block ID 1638727749, a distance of 0.9° from the phase centre.

The remaining targets had no other archival data available, and thus we pursued targeted observation with the upgraded Giant Metrewave Radio Telescope (uGMRT; Swarup et al. 1991; Gupta et al. 2017) and the Five-hundred-meter Aperture Spherical Telescope (FAST; Nan et al. 2011) for northern hemisphere targets, and MeerKAT for southern hemisphere targets. We present summaries of all HI observations in Table 2.

https://doi.org/10.1017/pasa.2025.10123 Published online by Cambridge University Press

Table 2. Summary of FRB host galaxy HI observations.

FRB	Facility	Observation Date(s)	Channel Width (kHz)[a]	Time On Source (mins)	Bandpass Calibrator	Gain Calibrator
FRB 20181220A	GMRT	17/19th August 2024	24.414	996	3C286	2202+422
	FAST	30th September 2024	7.629	10	-	-
FRB 20181223C	GMRT	17/19/23rd August 2024	24.414	1038	3C147	1158+248
	FAST	21st Decemeber 2024	7.629	51	-	-
FRB 20190418A	GMRT	16/17/21st August 2024	48.828	1056[b]	3C48	0421+206
FRB 20190425A	GMRT	22/26/27th August 2024	24.414	990	3C286	1640+123
	FAST	8th February 2025	7.629	3	-	-
FRB 20200223B	GMRT	10/18/23rd November 2023	48.828	1020	3C48	0029+349
	FAST	1st October 2024	7.629	1	-	-
FRB 20200723B	MeerKAT	17th December 2022	208.984	30	J1939-6342	J1215-1731
FRB 20201123A	MeerKAT	12th January 2021	208.984	60	J1939-6342	J1744-5144
FRB 20210405I	MeerKAT	21st June 2024	13.062	240	J1939-6342	J1744-5144
FRB 20211127I	MeerKAT	18th March 2023	3.265	180	J1939-6342	J1311-2216
FRB 20211212A	MeerKAT	13th December 2022	3.265	180	J0408-6545	J1008+0730
FRB 20231229A	Arecibo[c]	-	24.390	∼1	-	-
FRB 20231230A	MeerKAT	5th December 2021	208.984	450	J0408-6545	J0503+0203
FRB 20240201A	MeerKAT	21st February 2025	26.123	240	J0408-6545	J1008+0730
	FAST	13th November 2024	7.629	23	-	-
FRB 20240210A	MeerKAT	28th July 2025	26.123	240	J0408-6545	J0025-2602
FRB 20240312D	MeerKAT	29th June 2025	26.123	240	J0408-6545	J0303-6211
FRB 20240615B	MeerKAT	3rd August 2025	26.123	240	J0408-6545	J0240-2309
FRB 20250316A	Effelsberg[d]	Oct/Nov 1989	11.965	-	-	-

a Raw observation channel widths; we rebin to lower resolution in most cases.
b 16th August observation is corrupted, true on source time is ∼66% of this.
c Haynes et al. (2018) - ALFALFA survey was conducted over a 7 year time span with an average integration time of 48 seconds.
d Haynes et al. (1999) - precise on source time unknown.

2.2.1 *GMRT Observations and Data Reduction*

Through proposals 45_059 and 46_112, we obtained a total of 114 hours of *L* band observation (∼85 hours on-source) centred on the hosts of FRB 20181220A, FRB 20181223C, FRB 20190418A, FRB 20190425A (Bhardwaj et al. 2024) and FRB 20200223B (Ibik et al. 2023). These observations were taken in November 2023 and August 2024, using the GMRT Wideband Backend as the correlator. Depending on the location of the HI line in the band, we used 100 MHz and 200 MHz bandwidths between 1260 - 1460 MHz, covering the entire $z = 0 - 0.1$ range. These were subdivided into 4096 channels, resulting in velocity resolutions of ~ 6 km s^{-1} and $\sim$12 km s^{-1} respectively.

The raw data were transferred and processed using CASA (McMullin et al. 2007) on the `ilifu` supercomputing cloud system. Initial flagging of corrupted antennas and scans was completed manually, and gain, bandpass, and phase calibrations were conducted following standard procedures. The data were rebinned to 1 MHz for self-calibration, and the calibration solutions were applied to the visibilities around the HI line region. Final deep continuum images were made out to the first null of the uGMRT primary beam, whose resulting model continuum visibilities were subtracted from the corrected visibilities using the CASA task UVSUB. The residual data were then run through a final round of automatic RFI removal.

A uv-plane continuum subtraction was completed with the CASA task UVCONTSUB, excluding 500 km s^{-1} around the region of the HI line with a first order polynomial fit. We then made data cubes surrounding the host galaxy coordinates using the CASA task TCLEAN with Briggs weighting. Various robust levels and resolutions were employed to test different emphases on sensitivity and structure, ensuring that around 5 pixels covered the beam. Due to some residual variations in the baseline, in a few cases we ran a final image-plane based continuum subtraction using the CASA task IMCONTSUB, excluding the channels visibly containing HI emission with a second order polynomial. Finally, each spectral-line datacube was corrected for its frequency-dependent primary beam shape and convolved to its largest synthesised common beam.

2.2.2 *MeerKAT Observations and Data Reduction*

Through three MeerKAT proposals (project IDs SCI-20220822-MG-01, SCI-20230907-MG-02 and SCI-20241103-MG-01), we obtained a total of 14 on-source hours, centred on the hosts of seven FRBs. The observations were conducted from December 2022, through to August 2025 (capture block IDs 1670970986, 1679181682, 1718998942, 1739386395, 1740164485, 1751156931, 1753661382, and 1754260765). Each observation was taken in the *L* band (107 MHz centred at 1358.5 MHz) at

https://doi.org/10.1017/pasa.2025.10123 Published online by Cambridge University Press

32K and 32K-zoom spectral resolutions, which corresponds to velocity resolutions of 5.5 km s^{-1} and 0.7 km s^{-1} respectively.

The data were stored on `ilifu` and processed using `PROCESSMEERKAT`[a], a dedicated MeerKAT reduction pipeline which also utilises CASA. We rebinned the 32K-zoom data to a maximum of 64 K mode (i.e. 13.062 kHz wide channels) for this step.

Model continuum visibilities were subtracted from the corrected data using UVSUB, and then a further UVCONTSUB step was run. Spectral-line cubes were made using TCLEAN with Briggs weighting, again with various robust levels, resolutions, and cleaning depths. Each cube was primary beam corrected using `katbeam`[b] and then was convolved to a synthesised common beam.

2.2.3 FAST Observations and Data Reduction

To supplement a few northern hemisphere observations, and in reaction to more recent FRB localisations, we proposed for FAST time through proposal SQB-2024-0174 and were awarded four hours of observation. The targets were observed in On-Off mode with the spec(W+N) backend; this spectral backend records the full 400 MHz (1.05-1.45 GHz) bandwidth with a resolution of 7.629 kHz, and a narrower 31.25 MHz region with a resolution of 476.83 Hz. The On-Off mode utilises the periodic injection of a standardised noise diode for flux calibration.

The data are stored in FITS format as a dual polarisation time series of bandwidth data. We separated the on and off source data and performed a temperature calibration using the high power noise diode (e.g. Section 3.1 of Jing et al. 2023) to convert from raw power to brightness temperature. Due to the electromagnetic wave reflection that is common in single dish instruments, the FAST data contains periodic fluctuations in the bandpass which manifest as standing waves. We removed this signal using a fast Fourier transform (FFT) based approach, modelled off the methods of Xu et al. (2024). Using the spectroscopic redshifts of each target, we extracted 2000 km s^{-1} around the HI line and stacked each observation weighted by its RMS noise.

To subtract the baseline, we performed a polynomial fit with 250 km s^{-1} excluded around the HI frequency. The polynomial was chosen as either 3rd or 4th degree such that the resulting baseline was flat around the line. In a few datasets, the baseline was too erratic for a clean subtraction; for these cases we first subtracted the off source summed spectra from the on source summed spectra, and then performed the baseline polynomial fitting. This was completed separately for each polarisation, and the final spectra was obtained by stacking them together.

3. HI Results

Here we highlight the global HI properties of the sample. For each spatially resolved observation (i.e., the GMRT and MeerKAT datacubes), we use the SoFiA-2 (Westmeier et al. 2021) source finding pipeline to extract HI sources and generate moment maps. We use the pipeline's default smooth-and-clip (S+C) finder with parameters following those used in T. Westmeier et al. (2022) for the pilot data release of the WALLABY survey (which SoFiA-2 was designed for). This includes a `scfind.threshold` value of 3.5 and a `reliability.minSNR` value of 3, to ensure only robust signals are picked up. For detections with particularly narrow line widths, we rerun SoFiA-2 with a maximum spectral axis smoothing kernel equal to this apparent width.

Figure 1 presents spectra for each target, binned to lower spectral resolution where sensible[c]. The GMRT and MeerKAT spectra are generated by summing the flux from pixels included in a 2D mask, which itself is a flattened projection of the 3D mask generated by SoFiA-2. We also present moment 0 (intensity), moment 1 (velocity), and moment 2 (velocity dispersion) maps for these targets in Figure 2, overlaid on imaging from the DESI Legacy Imaging Survey (Dey et al. 2019), the Dark Energy Camera Plane Survey (Saydjari et al. 2023, DECaPS), and the Pan-STARRs1 survey (Chambers et al. 2016). The lowest contours are defined as the 3σ level measured by SoFiA-2[c].

Table 3 presents a summary of the global HI properties of the sample. These properties are measured from the masked spectra; i.e. only voxels in the 3D SoFiA-2 mask are included, and as a result they are slightly different to those displayed in Fig. 1. We calculate HI masses following Meyer et al. (2017, equation 48), assuming a 10% absolute flux scale uncertainty on all measurements due to calibration alongside the noise contribution. As radio continuum (RC) emission is considered a robust tracer of star formation due to its association with young, massive stars, when RC sources are present, we estimate an SFR following the methods of Molnar et al. (2021, equation 22).

We estimate the radius of the HI emission, $R_{\rm HI}$, out to the 3σ contour level by measuring the average surface density[c] of the intensity maps as a function of elliptical radius from a chosen centre, which we choose to be the optical centre of brightness in the survey imaging. This $R_{\rm HI}$ estimate is technically a lower limit; as many of our maps do not reach the nominal 1 $M_\odot$pc^{-2} threshold used in the literature, they are not necessarily half the disk size $D_{\rm HI}$ commonly used to describe HI disks e.g. for the mass-size relation (Wang et al. 2016). We estimate the ellipticity and position angles of the galaxies using 2MASS (Skrutskie et al. 2006) K-band data where possible; otherwise we fit elliptical isophotes to the legacy photometry presented in Fig. 2. These values are then combined with estimates of the galaxies' rotation velocities $V_{\rm rot}$ to make broad approximations of the dynamical mass $M_{\rm dyn}$ and hence the virial mass M_{200} for these galaxies. We estimate $V_{\rm rot}$ using

$$V_{\rm rot} = \frac{W_{50}}{2 \sin i}$$

where W_{50} is the line width at 50% of the peak flux and

a. https://idia-pipelines.github.io/docs/processMeerKAT
b. https://github.com/ska-sa/katbeam

c. See Table 5 in Appendix for more information.

https://doi.org/10.1017/pasa.2025.10123 Published online by Cambridge University Press

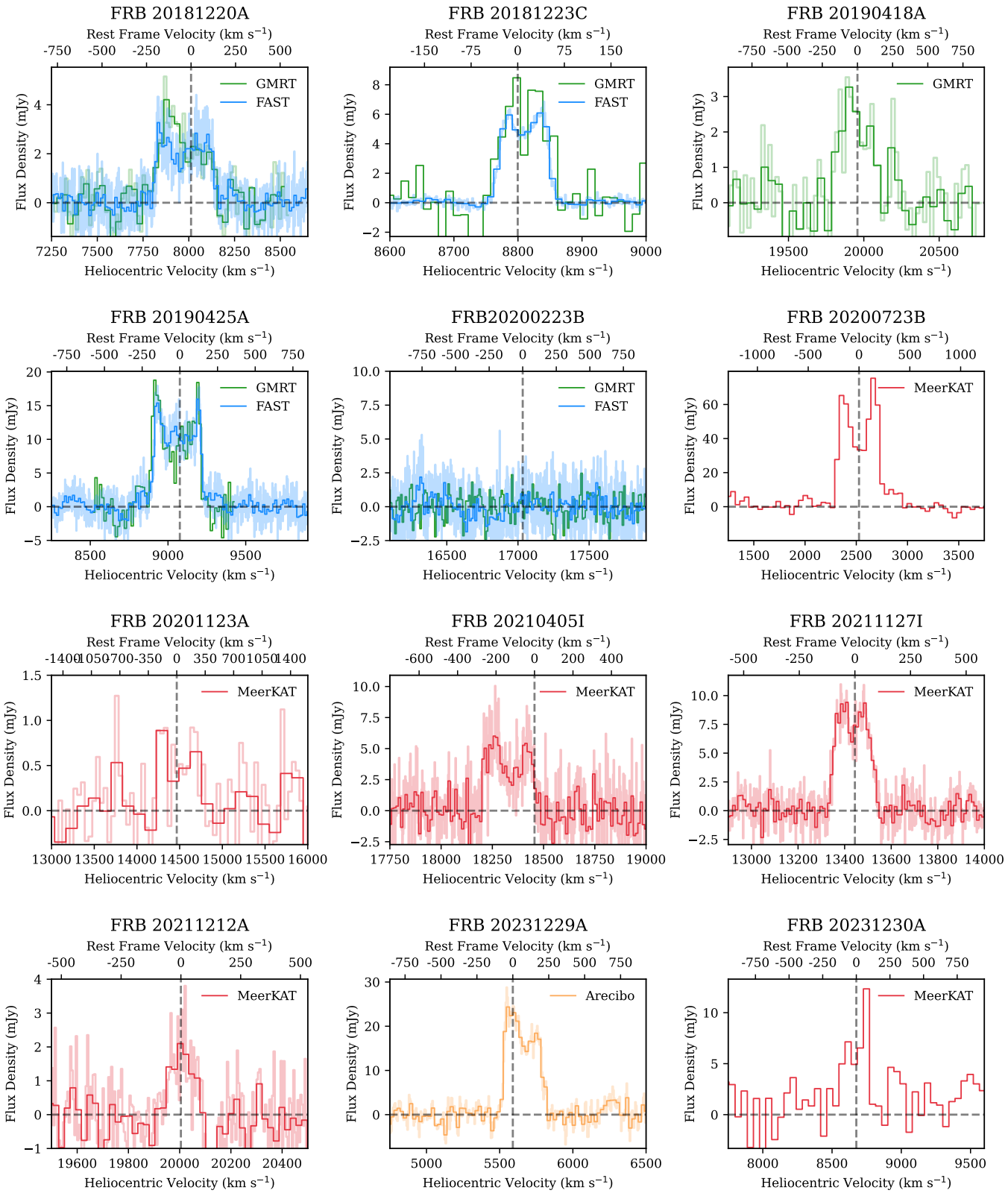

Figure 1. HI spectra of the FRB host galaxies. The red, green, and blue colours represent dedicated observations from FAST, GMRT, and MeerKAT, with the two orange spectra taken from archival data. When necessary, the data are binned by various channel widths; fainter lines in the plots represent the raw data, with bolder lines representing the binned data. The vertical dashed line represents the rest frame of the hosts', determined by their optical redshifts.

https://doi.org/10.1017/pasa.2025.10123 Published online by Cambridge University Press

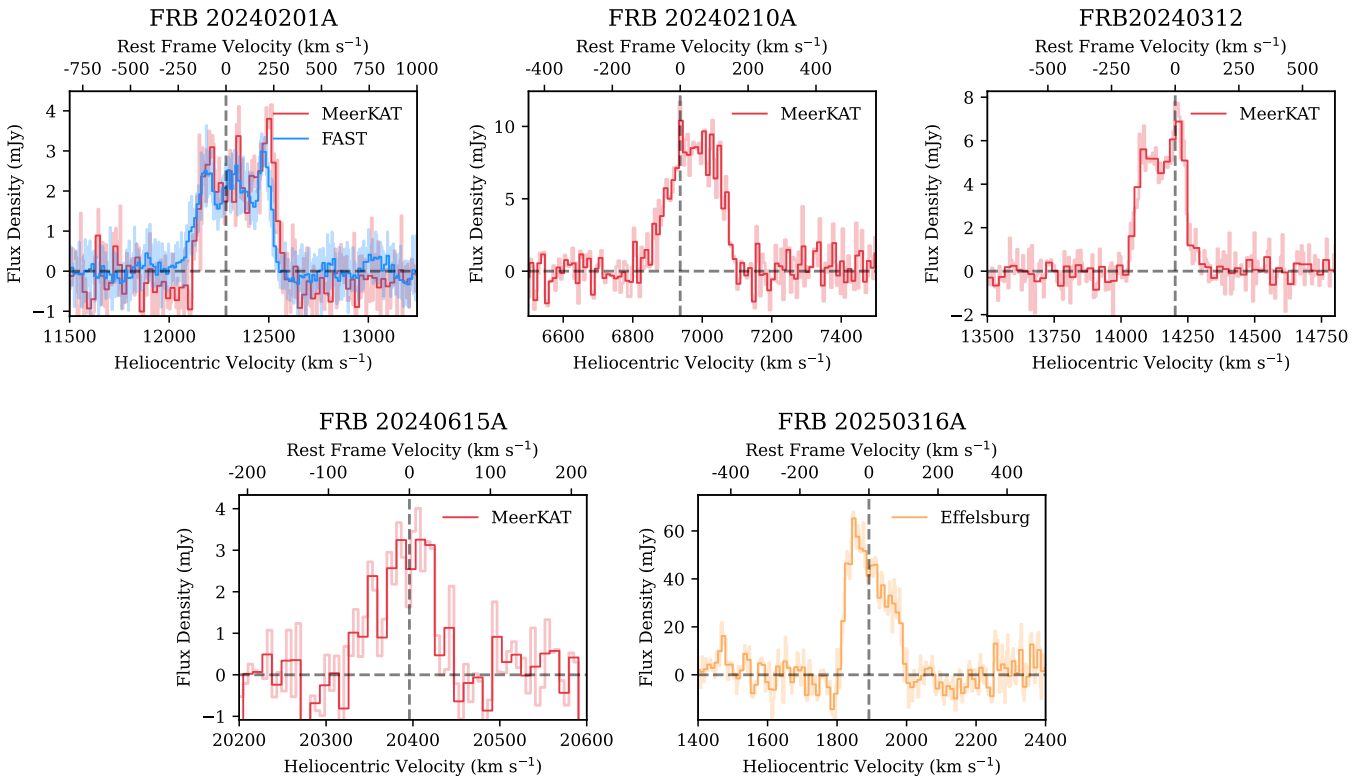

Figure 1. FRB host galaxy HI spectra (continued)

i is the inclination of the galaxy; we discard four galaxies with inclinations lower than 10°. To ensure these rotational velocities are in the flat part of each galaxies' rotation curve, we examine position-velocity diagrams across the major axes and find that all targets extend beyond the break. We do not apply systematic corrections for instrumental broadening and turbulence as we expect such corrections to be small for such high resolution data, and we are not attempting a fully robust measurement. We calculate $M_{\rm dyn}$ and M_{200} following Yu, Ho, and Wang (2020, equations 10 & 13).

3.1 Marginal / Non-Detections

As seen in Fig. 1, the host of FRB 20201123A peaks very marginally above the noise. This host is at a relatively high redshift of 0.0507, and the MeerKAT observation was 0.4° from the phase centre. Due to this, and the beam size, we presume the picked-up signal is simply the unresolved core emission; as such, we do not place much weight on its derived HI properties, considering its HI mass to be a lower limit. Only its intensity map is displayed in Fig. 3, and we do not attempt to measure its asymmetry.

Fig. 1 also shows the non-detection of the host of FRB 20200223B. We place a 5σ upper limit on its HI mass using both the GMRT and FAST data, assuming a linewidth of 200 km s^{-1} and a disk size of 30 kpc. As outlined in Ibik et al. (2023), this host is in a transitional regime between star-formation and quiescence, which reflects its lower gas fraction. This is uncommon for FRB hosts; Gordon et al. (2023) and Sharma et al. (2024) clearly find a preference towards star-forming galaxies, a conclusion well supported by our findings given that 16 of our 17 targets are emitting in HI.

4. Asymmetry Calculations

To fully investigate the degree of disturbance in the HI distributions of FRB hosts, we employ close by-eye examination of the spectral profiles, the moment maps, and individual channel intensity maps. However, we also wish to quantify any disturbance to allow for direct comparison with background galaxies. In this section, we cover our methods for quantifying and calculating the asymmetry of the HI detections.

4.1 Asymmetry Metrics

There are a number of common metrics used in the literature to assess asymmetry (see the introduction of Deg et al. 2023, for an overview); in this study we utilise five: $A_{\rm flux}$, $A_{\rm spec}$, $A_{\rm 1D}$, $A_{\rm 2D}$, and $A_{\rm 3D}$. The first is a common historical measurement used to consider the lopsidedness of a spectrum, and is defined by

$$A_{\rm flux} = \left| \max(F_{\rm l}/F_{\rm u}\ ,\ F_{\rm u}/F_{\rm l}) \right| \qquad (1)$$

where

$$F_{\rm l} = \int_{\nu_1}^{\nu_{\rm sys}} F_\nu\, d\nu \qquad (2)$$

https://doi.org/10.1017/pasa.2025.10123 Published online by Cambridge University Press

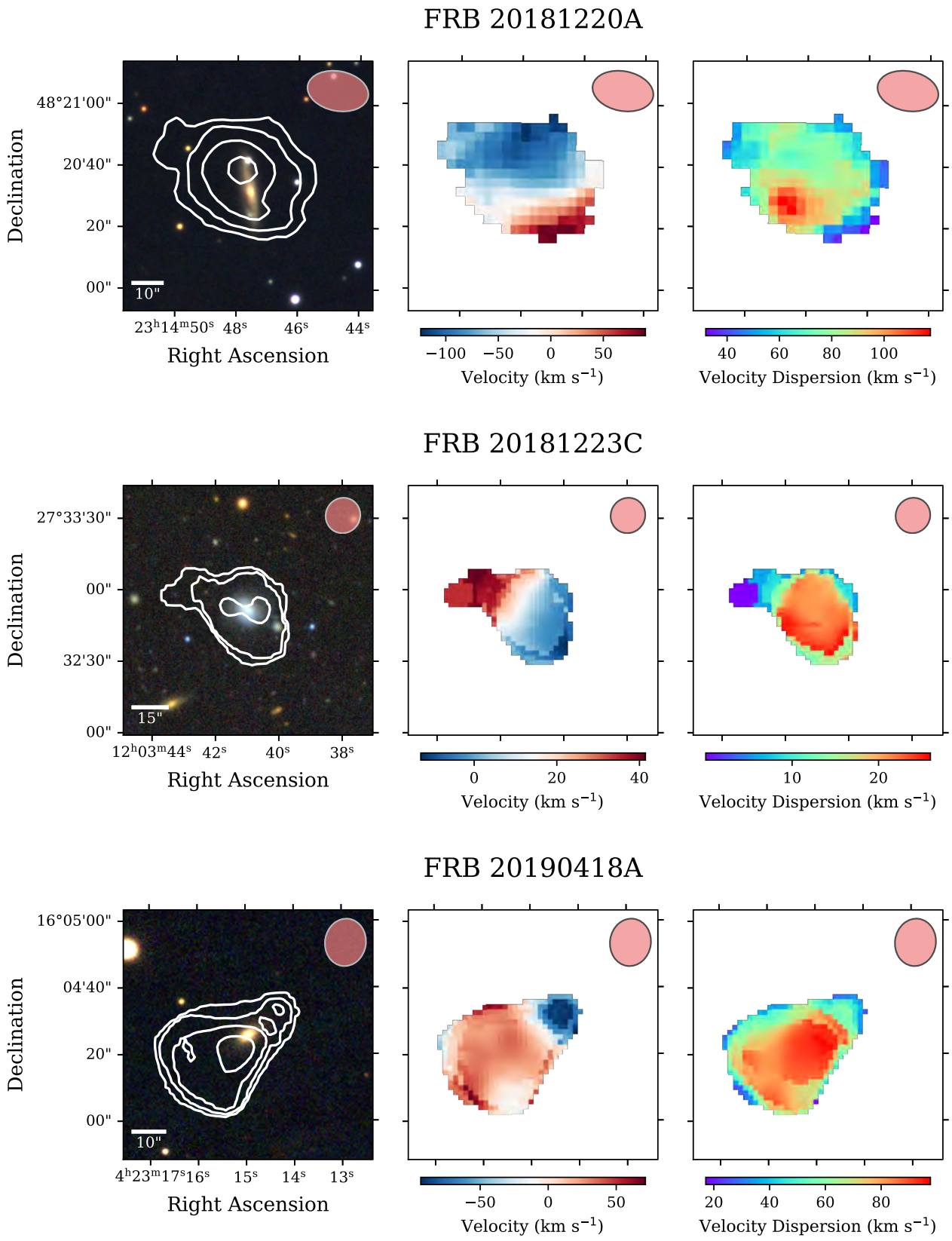

Figure 2. FRB host galaxy moment maps, displaying total intensity (left), velocity (centre) and velocity dispersion (right). The lowest contours are at the 3σ level, with the higher contours set at varying multiples of that level. When the FRB's localisation region is significantly smaller than the size of its host, we include its position shown in magenta in the intensity maps and black in the others; a star represents a localisation region too small to be shown, whereas a cross and dashed ellipse shows the estimated position and 1σ uncertainty region. The beam sizes are shown in the upper right hand corner. Velocities are displayed in the rest frame, defined with respect to the optical redshift.

https://doi.org/10.1017/pasa.2025.10123 Published online by Cambridge University Press

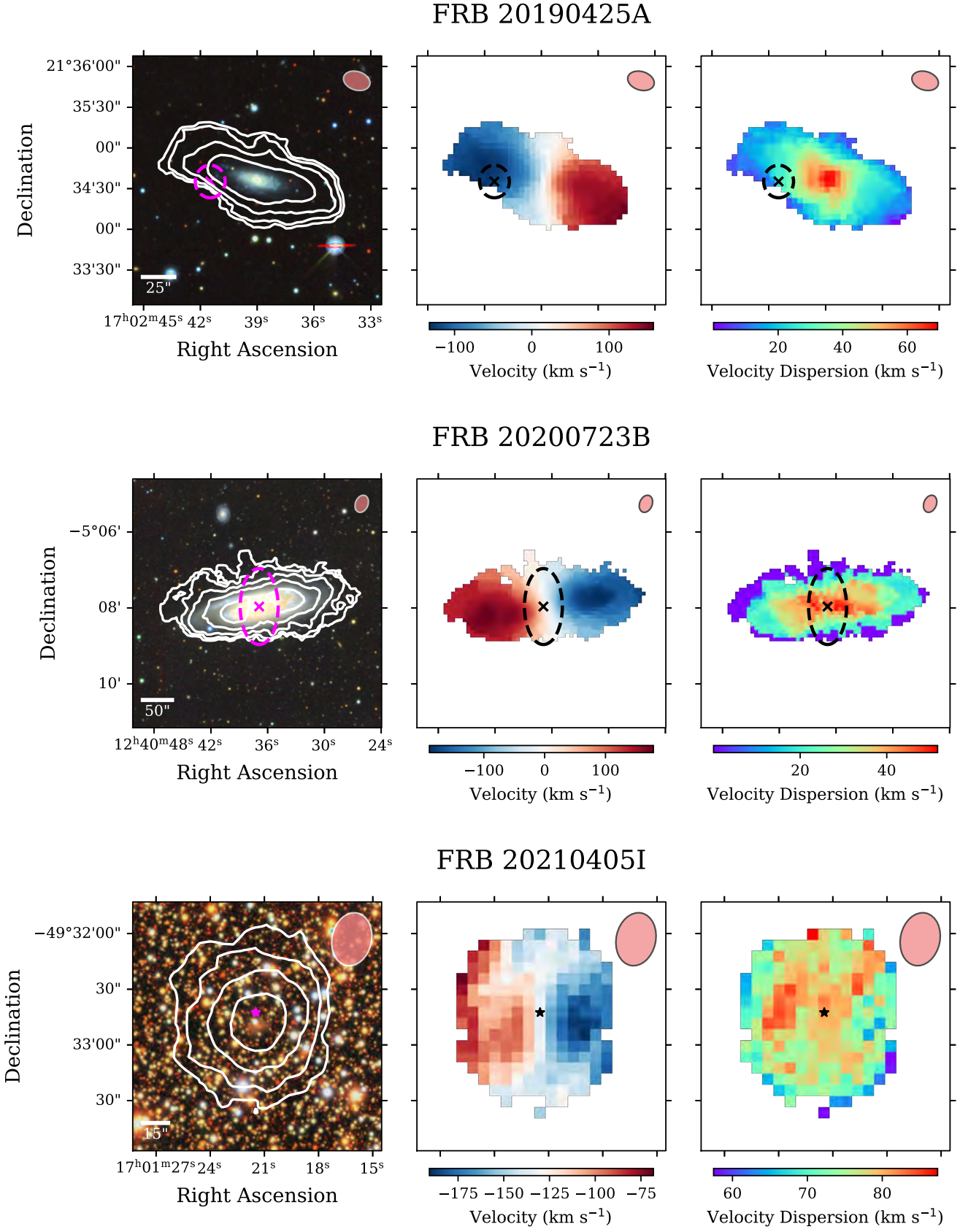

Figure 2. FRB host galaxy moment maps (continued).

https://doi.org/10.1017/pasa.2025.10123 Published online by Cambridge University Press

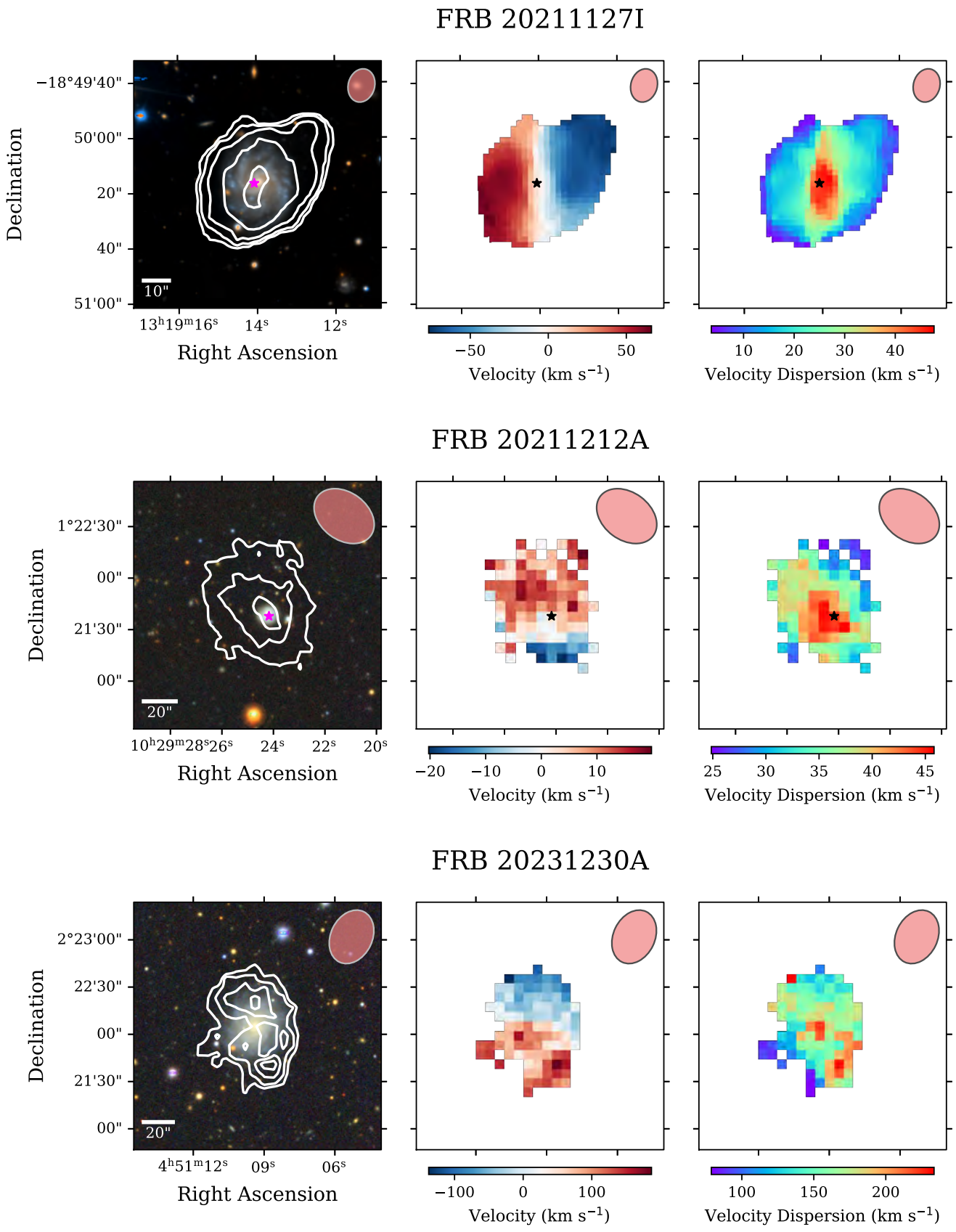

Figure 2. FRB host galaxy moment maps (continued).

https://doi.org/10.1017/pasa.2025.10123 Published online by Cambridge University Press

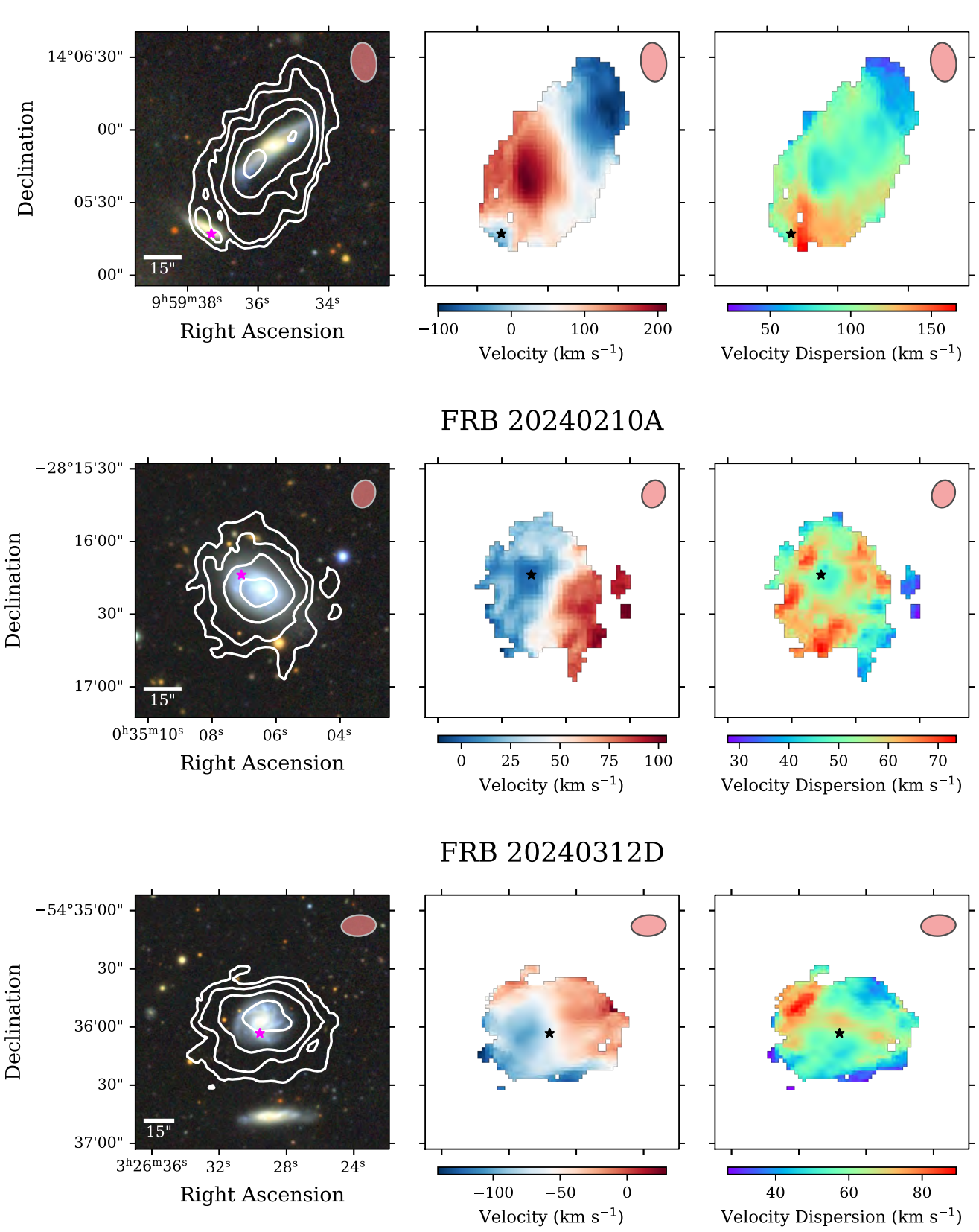

Figure 2. FRB host galaxy moment maps (continued).

https://doi.org/10.1017/pasa.2025.10123 Published online by Cambridge University Press

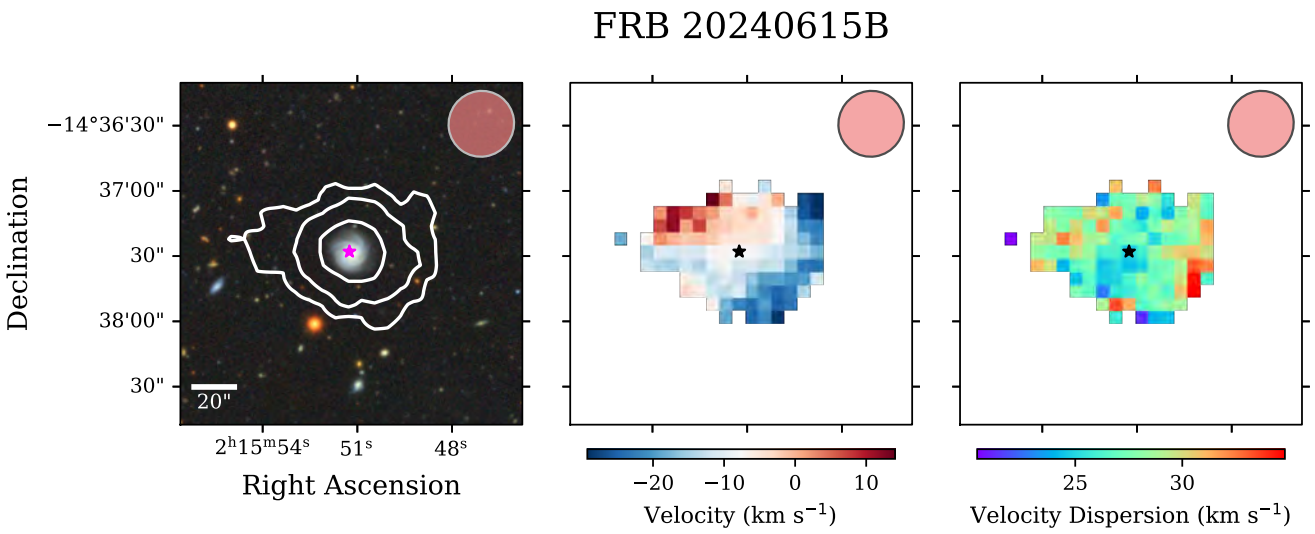

Figure 2. FRB host galaxy moment maps (continued).

Table 3. Host galaxies properties derived from radio observations: HI flux, HI mass, line width (defined by the width between the 50% peak flux levels), radio continuum flux density, radio-derived star formation rate, HI disk radius, and virial mass.

FRB Name	Observation	$S_{\rm HI}$ (Jy km s^{-1})	$\log(M_{\rm HI})$ ($M_\odot$)	$W50$ (km s^{-1})	$S_{\rm cont}$[a] (mJy)	SFR$_{\rm radio}$ ($M_\odot$ yr^{-1})	$R_{\rm HI}$ (kpc)	$\log(M_{200}/M_\odot)$[b]
FRB 20181220A	GMRT	0.76 ± 0.12	9.44 ± 0.08	126 ± 14	2.72	$2.29^{+1.30}_{-0.83}$	20.5 ± 10.0	11.0
	FAST	0.72 ± 0.08	9.42 ± 0.05	315 ± 2	N/A	N/A	N/A	N/A
FRB 20181223C	GMRT	0.60 ± 0.10	9.42 ± 0.08	70 ± 5	$\leq$0.08	$\leq$0.15	11.1 ± 2.4	10.6
	FAST	0.45 ± 0.04	9.30 ± 0.05	79 ± 1	N/A	N/A	N/A	N/A
FRB 20190418A	GMRT	0.82 ± 0.15	10.33 ± 0.09	217 ± 19	$\leq$0.06	≤ 0.51	36.2 ± 8.2	-
FRB 20190425A	GMRT	3.55 ± 0.39	10.22 ± 0.05	303 ± 3	1.11	$1.35^{+0.75}_{-0.48}$	35.0 ± 5.0	12.0
	FAST	3.61 ± 0.36	10.23 ± 0.05	307 ± 1	N/A	N/A	N/A	N/A
FRB 20200223B	GMRT	$\leq$0.13	$\leq$9.377	N/A	0.10	$0.59^{+0.32}_{-0.21}$	N/A	N/A
	FAST	≤ 0.14	≤ 9.394	N/A	N/A	N/A	N/A	N/A
FRB 20200723B	MeerKAT	20.47 ± 2.11	9.84 ± 0.05	401 ± 4	47.7	$3.42^{+1.97}_{-1.25}$	23.0 ± 2.9	12.0
FRB 20201123A	MeerKAT	0.41 ± 0.18	9.72 ± 0.16	415 ± 36	5.15	$10.9^{6.50}_{-4.08}$	N/A	N/A
FRB 20210405I	MeerKAT	1.00 ± 0.12	10.34 ± 0.06	245 ± 5	0.59	$2.85^{+1.63}_{-1.04}$	29.3 ± 3.3	12.7
FRB 20211127I	MeerKAT	0.90 ± 0.10	9.99 ± 0.05	158 ± 3	1.16	$2.82^{+1.61}_{-1.02}$	14.5 ± 2.5	11.7
FRB 20211212A	MeerKAT	0.17 ± 0.04	9.65 ± 0.11	87 ± 8	0.31	$1.92^{+1.09}_{-0.69}$	25.9 ± 9.0	-
FRB 20231229A	Arecibo	5.29 ± 0.54	9.96 ± 0.05	256 ± 3	N/A	N/A	N/A	N/A
FRB 20231230A	MeerKAT	0.18 ± 0.04	8.89 ± 0.09	206 ± 21	$\leq$5.19	$\leq$4.47	12.3 ± 3.4	-
FRB 20240201A†	MeerKAT	1.01 ± 0.11	9.96 ± 0.05	373 ± 5	0.42	$1.04^{+0.57}_{-0.37}$	-	-
	FAST	0.89 ± 0.09	9.90 ± 0.05	384 ± 1	N/A	N/A	N/A	N/A
FRB 20240210A	MeerKAT	1.51 ± 0.16	9.61 ± 0.05	166 ± 1	1.67	$1.19^{+0.66}_{-0.43}$	16.8 ± 4.2	11.38
FRB 20240312D	MeerKAT	1.25 ± 0.13	10.19 ± 0.05	182 ± 1	1.26	$3.31^{1.90}_{1.21}$	27.2 ± 4.3	-
FRB 20240615B	MeerKAT	0.25 ± 0.03	9.84 ± 0.06	76 ± 1	0.30	$1.99^{+1.12}_{-0.72}$	30.3 ± 3.0	11.39
FRB 20250316A	Effelsberg	7.13 ± 0.79	9.13 ± 0.05	132 ± 2	N/A	N/A	N/A	N/A

a Estimates are accompanied by 10% uncertainties due to absolute flux scaling errors.
b Dashes indicate hosts with inclinations too near 0 for proper $V_{\rm rot}$ correction.
† HI estimates include entangled neighbour emission.

is the integrated flux of the lower half of the spectrum up to some central velocity $v_{\rm sys}$, and

$$F_{\rm u} = \int_{v_{\rm sys}}^{v_2} F_v \, dv \tag{3}$$

https://doi.org/10.1017/pasa.2025.10123 Published online by Cambridge University Press

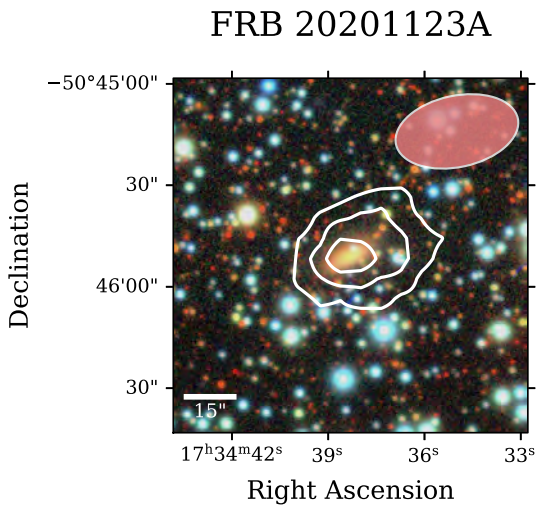

Figure 3. Intensity map of the unresolved detection of the host of FRB 20201123A.

is the integrated flux of the upper half. This central velocity is generally defined as the systemic velocity, given by the midpoint of the spectrum at the 20% flux level.

The second metric, $A_{\rm spec}$, was introduced by Reynolds et al. (2020) to emphasise more local disturbances through investigation of channel-by-channel variation, defined by

$$A_{\rm spec} = \frac{\sum_{i=1} | S(i) - S(i_{\rm flip}) |}{\sum_{i=1} | S(i) |} \quad (4)$$

where $S(i)$ and $S(i_{\rm flip})$ are the fluxes of the $i^{\rm th}$ channel and its mirrored channel pair about a central channel. This centre is generally different than $v_{\rm sys}$, and is instead chosen as the flux-weighted mean velocity to highlight the differences in profile far away from the centre of mass, e.g. through an extended tail on one side of the spectrum. These metrics were used in Michalowski (2021) and Glowacki et al. (2023) to compare FRB hosts with wider LVHIS and HALOGAS HI survey populations (Reynolds et al. 2020), and thus we include calculations here.

Recently, Deg et al. (2023) introduced new metrics to properly account for the bias contributed by noise to the asymmetry of a profile, and to take advantage of the full information that three-dimensional datacubes can offer. As next generation surveys, such as WALLABY and LADUMA, will resolve many HI galaxies, these higher dimensional metrics are likely to be the most robust way to quantify a galaxy's disturbance, especially in low SNR regimes. Thus, we also calculate values for $A_{\rm 1D}$, $A_{\rm 2D}$, and $A_{\rm 3D}$, based on equation 20 in Deg et al. (2023):

$$A_{\rm 1D/2D/3D} = \left(\frac{P_{\rm sq,m} - B_{\rm sq,m}}{Q_{\rm sq,m} - B_{\rm sq,m}} \right)^{1/2} \quad (5)$$

where

$$P_{\rm sq,m} = \sum_{i}^{N} (f_i - f_{-i})^2 \quad (6)$$

is the sum of the squared difference between each flux channel/pixel/voxel f_i in an HI profile and its mirrored counterpart f_{-i} about a 1D/2D/3D rotation point,

$$Q_{\rm sq,m} = \sum_{i}^{N} (f_i + f_{-i})^2, \quad (7)$$

and $B_{\rm sq,m}$ is the contribution of the noise to $P_{\rm sq,m}$, which for uncorrelated Gaussian noise σ can be approximated as $2N\sigma^2$. These metrics are calculated by the `3DACs` code[d], which simply requires a datacube, a source mask, and a 3D rotation voxel as inputs.

It should be noted that in some cases, $B_{\rm sq,m}$ may be larger than $Q_{\rm sq,m}$, which causes the result to be undefined. This indicates that the noise is dominating the measured asymmetry $P_{\rm sq,m}$. `3DACs` returns a value of -1 in these cases, which should be treated essentially equal to a value of zero.

The choice of rotation voxel is critical to the usefulness and applicability of these metrics. We want to define it such that tidal features cannot introduce bias in either the spatial or spectral dimensions. As such, we choose to first find the optical centre of brightness in the background survey image, and take the flux weighted centre of the spectrum at the closest pixel to this 2D point. This choice is thus sensitive to any gas volume that is away from the centre of the galaxy's core.

We note that as we cannot run `3DACs` on the single dish spectra, for consistency we calculate all $A_{\rm 1D}$ values externally (following the same methodology as above) using the flux weighted centre as the pivot. As `3DACs` estimates the RMS noise of the 1D spectrum based on an expected scaling of the 3D RMS noise when summing over spatial pixels, rather than measuring the noise itself, our values differ slightly, though never significantly.

When extracting final values for each of the 1D metrics, we consider the optimal spectral resolution. Each can become temperamental as the SNR of the HI line decreases and as the linewidth (in channels) decreases, and thus we take measurements at many different rebinning ratios (i.e. until the spectral line is unresolved) to estimate the most stable resolution. This estimation differs between target and is done purely by eye; we inspect the variation of each metric to find the resolution which appears coincident with the most overall stable point in the three metrics, aiming to use the highest resolution possible. We highlight an example case in Fig. 11 in the Appendix.

4.2 Asymmetry Thresholds

We wish to identify the thresholds above which a profile is considered asymmetric for each of our metrics. Espada et al. (2011) modelled the $A_{\rm flux}$ distribution of AMIGA isolated galaxies, finding a 2σ threshold of 1.26. Reynolds et al. (2020) did the same with the low density fields of LVHIS and HALOGAS, and the higher density field of VIVA, finding 2σ thresholds of 1.25, 1.17, and 1.53 respectively for galaxies with stellar masses $\geq 10^9\ M_\odot$. Watts et al. (2020) focused on the more

d. https://github.com/NateDeg/3DACS

https://doi.org/10.1017/pasa.2025.10123 Published online by Cambridge University Press

representative xGASS sample, and chose to define asymmetry by generating noiseless mock spectra with inherent $A_{\rm flux}$ equal to 1.1, perturbing them by various noise levels, and finding the threshold (as a function of SNR) within which 80% of the spectra are measured. Considering these results and the fact that a number of our targets are low SNR (<10), we choose a flat threshold of 1.3; this is similar to the 3σ limits of Espada et al. (2011) and Reynolds et al. (2020), and corresponds to the low SNR threshold of Watts et al. (2020).

Reynolds et al. (2020) also measured $A_{\rm spec}$ for the LVHIS, HALOGAS, and VIVA samples, finding 2σ thresholds of 0.428, 0.263, and 2.031 respectively. As this metric is the most affected by noise, we choose a slightly arbitrary conservative threshold of 0.5; this also reflects the fact that FRB hosts are not exclusively found in low-density environments.

As the $A_{\rm 1D}$, $A_{\rm 2D}$, and $A_{\rm 3D}$ measurements are even newer, there are not many comparisons to be made with wider populations from which to infer at what point a profile is considered asymmetric. Perron-Cormier et al. (2025) recently applied these metrics to data from the WALLABY pilot survey (T. Westmeier et al. 2022) and found that an $A_{\rm 3D}$ threshold of 0.5 corresponds to highly disturbed galaxies, though this value likely represents the extreme end of the disturbance spectrum. Fig. 8 of Deg et al. (2023) presents a trial analysis of 500 galaxies from a simulated WALLABY-like survey, showing a median visual disturbance of approximately 0.2, with most values falling within 0.1 of this median. Thus, an $A_{\rm 3D}$ value of 0.3 can serve as a rough threshold for identifying galaxies with above-average disturbance. In Section 5, we also present asymmetry measurements of the disturbed FRB host from Lee-Waddell et al. (2023) to use as a reference.

4.3 Uncertainties

The uncertainties in the 1D metrics come from a number of sources; we first consider statistical contributions arising from the inherent noise component of each channel. We estimate this statistical uncertainty following Michalowski (2021) and Glowacki et al. (2023). We take the standard deviation of the line-free regions of the spectra at their final chosen resolutions, and remeasure each metric 1000 times with the spectra shifted by a noise array generated by a Gaussian of this width. The final uncertainties are taken as the standard deviation of these measurements.

There are also a number of contributors to the systematic uncertainty that arises from these methodologies. One source originates from the choice of central velocity used in each of the metrics. As these centres are generally some fractional distance inside a channel, we must interpolate our spectral bins such that the nearest half channel increment aligns with the centre. We estimate the uncertainty in this method in a similar fashion as the statistical contribution, taking 1000 measurements with central velocities drawn from a Gaussian with a mean equal to the true centre and a width of one channel. The standard deviation of these results are taken as our systematic uncertainty. Thus, in our results, we present the value $\pm$ δ(stat.) $\pm$ δ(sys.)

The `3DACs` code does not output any uncertainties directly. Deg et al. (2023) claims that in their testing, the uncertainty associated with noise variation rarely exceeds 0.02, and almost certainly is dominated by systematics. We also note that the authors highlight imprecisions in the `3DACs` results when the size of the HI disk is smaller than four resolution elements (beams). Unfortunately, only three of our targets (FRB 20190425A, FRB 20200723B, and FRB 20211127I) satisfy this requirement. However, we still wish to investigate how useful these metrics are on real datasets across different instruments and resolutions. Thus, we choose to incorporate our own uncertainty associated with the choice of rotation centre — which is the quantity that introduces the most error due to low spatial resolution — by again retaking 1000 measurements with centres perturbed by a 3D Gaussian, with $\sigma_{\rm x}$, $\sigma_{\rm y}$, and $\sigma_{\rm v}$ all equal to 1. This is relatively straightforward as `3DACs` already incorporates interpolation methods to allow for fractional rotation centres. While a Gaussian of this width likely overestimates the uncertainty, it is simple in design and clearly accounts for the effect of spatial and spectral resolution. Furthermore, as we do not present a statistical contribution, we are satisfied with the larger systematic estimate.

There are also uncertainties that arise due to the effects of galaxy inclination and viewing angle. While Deg et al. (2020) clearly shows that both have notable impacts on these measurements, we do not incorporate such considerations here as their contributions are nontrivial to model and likely require detailed kinematic modelling to accurately describe.

5. Target Analysis

Here we discuss the asymmetry results for each FRB host galaxy, highlighting interesting cases. Table 4 presents the quantified asymmetry metrics for each target; at the bottom, we include measurements for the known disturbed host of FRB 20171020A (Lee-Waddell et al. 2023) to compare against.

5.1 FRB 20181220A

The host of FRB 20181220A is a highly inclined edge-on spiral which shows moderate HI emission in both the GMRT and FAST data. By eye, the higher SNR FAST spectrum appears largely symmetric, which is reflected in its low asymmetry metrics. In contrast, the GMRT spectrum exhibits significantly greater asymmetry, though the deviation is consistent within the noise level. Furthermore, the intensity map shows a peak line flux away from the optical core of the galaxy. This causes the $A_{\rm 2D}$ and $A_{\rm 3D}$ values to inflate to the highest in this sample. However, the area of the GMRT detection with respect to the beam size is right in the grey area of where Deg et al. (2023) identifies that 3D asymmetry modelling becomes less robust. Thus, we are hesitant to place too much weight on the GMRT result, especially considering the spectrum deviates from the FAST spectrum. The GMRT data does reveal that the galaxy lies in an HI rich group, with at least two other nearby detections in the field, the nearest of which lies 0.55 Mpc away.

https://doi.org/10.1017/pasa.2025.10123 Published online by Cambridge University Press

Table 4. Asymmetry measurements derived from HI profiles and moment maps: flux asymmetry (A_{flux}), spectral asymmetry (A_{spec}), one-dimensional morphological asymmetry (A_{1D}), two-dimensional map asymmetry (A_{2D}), and three-dimensional asymmetry (A_{3D}). For the first three columns, the first uncertainty represents the contribution from noise, and the second represents the contribution from resolution. For A_{2D} and A_{3D}, the uncertainties represent the choice of central rotation pixel/voxel.

FRB Name	Observation	A_{flux}	A_{spec}	A_{1D}	A_{2D} †	A_{3D} †
FRB 20181220A	GMRT	$1.504 \pm 0.649 \pm 0.528$	$0.354 \pm 0.170 \pm 0.168$	$0.161 \pm 0.098 \pm 0.078$	0.279 ± 0.086	0.463 ± 0.132
	FAST	$1.055 \pm 0.052 \pm 0.046$	$0.217 \pm 0.046 \pm 0.023$	$0.090 \pm 0.032 \pm 0.015$	N/A	N/A
FRB 20181223C	GMRT	$1.146 \pm 0.271 \pm 0.232$	$0.395 \pm 0.158 \pm 0.127$	$0.196 \pm 0.030 \pm 0.067$	0.259 ± 0.055	0.252 ± 0.097
	FAST	$1.084 \pm 0.044 \pm 0.073$	$0.229 \pm 0.036 \pm 0.102$	$0.112 \pm 0.022 \pm 0.057$	N/A	N/A
FRB 20190418A	GMRT	$1.302 \pm 0.375 \pm 0.397$	$0.488 \pm 0.177 \pm 0.168$	$0.224 \pm 0.035 \pm 0.099$	0.208 ± 0.041	0.232 ± 0.114
FRB 20190425A*	GMRT	$1.086 \pm 0.081 \pm 0.062$	$0.175 \pm 0.067 \pm 0.109$	$0.109 \pm 0.003 \pm 0.080$	0.099 ± 0.028	0.140 ± 0.062
	FAST	$1.054 \pm 0.029 \pm 0.027$	$0.171 \pm 0.022 \pm 0.028$	$0.070 \pm 0.016 \pm 0.029$	N/A	N/A
FRB 20200723B*	MeerKAT	$1.198 \pm 0.058 \pm 0.137$	$0.111 \pm 0.037 \pm 0.142$	$0.058 \pm 0.023 \pm 0.091$	0.084 ± 0.037	0.210 ± 0.166
FRB 20210405I	MeerKAT	$1.135 \pm 0.148 \pm 0.069$	$0.300 \pm 0.099 \pm 0.076$	$0.170 \pm 0.026 \pm 0.042$	0.074 ± 0.066	-
FRB 20211127I*	MeerKAT	$1.034 \pm 0.060 \pm 0.061$	$0.105 \pm 0.056 \pm 0.097$	$0.043 \pm 0.037 \pm 0.060$	0.091 ± 0.026	0.116 ± 0.042
FRB 20211212A	MeerKAT	$1.244 \pm 0.563 \pm 0.299$	$0.371 \pm 0.222 \pm 0.143$	$0.140 \pm 0.048 \pm 0.065$	0.126 ± 0.055	-
FRB 20231229A	Arecibo	$1.360 \pm 0.079 \pm 0.125$	$0.323 \pm 0.051 \pm 0.042$	$0.140 \pm 0.027 \pm 0.026$	N/A	N/A
FRB 20231230A	MeerKAT	$2.394 \pm 1.252 \pm 1.161$	$0.311 \pm 0.225 \pm 0.158$	$0.130 \pm 0.046 \pm 0.104$	-	-
FRB 20240210A*	MeerKAT	$1.048 \pm 0.057 \pm 0.035$	$0.197 \pm 0.053 \pm 0.055$	$0.077 \pm 0.016 \pm 0.035$	0.134 ± 0.063	0.166 ± 0.048
FRB 20240312D*	MeerKAT	$1.161 \pm 0.087 \pm 0.141$	$0.145 \pm 0.054 \pm 0.097$	$0.072 \pm 0.033 \pm 0.058$	0.133 ± 0.017	0.199 ± 0.059
FRB 20240615B	MeerKAT	$1.208 \pm 0.226 \pm 0.149$	$0.379 \pm 0.123 \pm 0.037$	$0.153 \pm 0.088 \pm 0.024$	0.053 ± 0.050	-
FRB 20250316A	Effelsberg	$1.659 \pm 0.187 \pm 0.192$	$0.406 \pm 0.081 \pm 0.015$	$0.180 \pm 0.049 \pm 0.008$	N/A	N/A
FRB 20171020A*	ATCA	$1.320 \pm 0.037 \pm 0.184$	$0.319 \pm 0.027 \pm 0.076$	$0.1633 \pm 0.013 \pm 0.036$	0.123 ± 0.016	0.237 ± 0.021

† Dashed lines indicate measurements with no statistically significant asymmetry (-1 result returned by 3DACs).
∗ Targets with resolutions / SNRs great enough for 2D/3D measurements to be considered robust according to Deg et al. (2023).

5.2 FRB 20181223C

The spiral host of FRB 20181223C clearly exhibits a disturbed HI distribution in the GMRT intensity map. Once again, the GMRT and FAST spectra do not fully match, but are consistent within the noise when accounting for the much lower SNR of the GMRT detection.

The moment 0 and 1 maps show a clear extension to the west, captured primarily in a single channel due to the low spectral resolution of the cube. To highlight this, we produce individual channel maps in Figure 4, with the channel at 8775 km s^{-1} revealing strong HI emission centred nearly 30" from the core of the galaxy. This is the primary cause of the higher A_{2D} and A_{3D} values exhibited by this target. We also note the interesting extension in the channel map at 8740 km s^{-1}, which is too faint to affect the total intensity map.

This host is clearly significantly disturbed, though the origin of this morphology is difficult to ascertain. There are a number of galaxies in the visual field, including one very nearby to the south east, and another further away to the west. However, Bhardwaj et al. (2024) investigated these as potential hosts of the FRB, and found incompatible redshifts greater than 0.25 for both. Thus, there is no clear candidate that could be causing a disturbance through tidal means.

5.3 FRB 20190418A

With the third most distant redshift in this sample, the massive host of FRB 20190418A exhibits a weak HI signal in the GMRT data. As such, its spectral features are largely dominated by the noise. However, the moment maps of Fig. 2 reveal an asymmetry in the extent of the galaxy either side of its core which gets picked up by SoFiA-2 even with a higher S+C threshold of 5. Furthermore, the asymmetry metrics all suggest disturbance; A_{flux} exceeds our threshold, A_{spec} is the highest in this sample, and even A_{1D} — which is the most resilient to noise — is also the highest in this sample. Thus, we consider this target disturbed, though deeper observations would be useful to confirm the nature of this.

5.4 FRB 20190425

The host of FRB 20190425A appears to be largely undisturbed. The FAST and GMRT spectra are symmetric, and the moment maps are typical for a spiral of this inclination. This is reflected in the low asymmetry metrics across the board, all of which are robust due to the spectral and spatial resolution of the cube. This galaxy also appears isolated, with no nearby HI detections observed.

5.5 FRB 20200723B

The host of FRB 20200723B again exhibits mostly typical HI emission, with a symmetrical spectrum and emission aligned with the plane of the optical disk. However, the northern edge of the galaxy appears a lot less smooth than the rest; investigating the individual channel maps reveals faint elongation in at least five channels out to approximately 20 kpc above the stellar disk, as shown in Fig. 5. To confirm the nature

https://doi.org/10.1017/pasa.2025.10123 Published online by Cambridge University Press

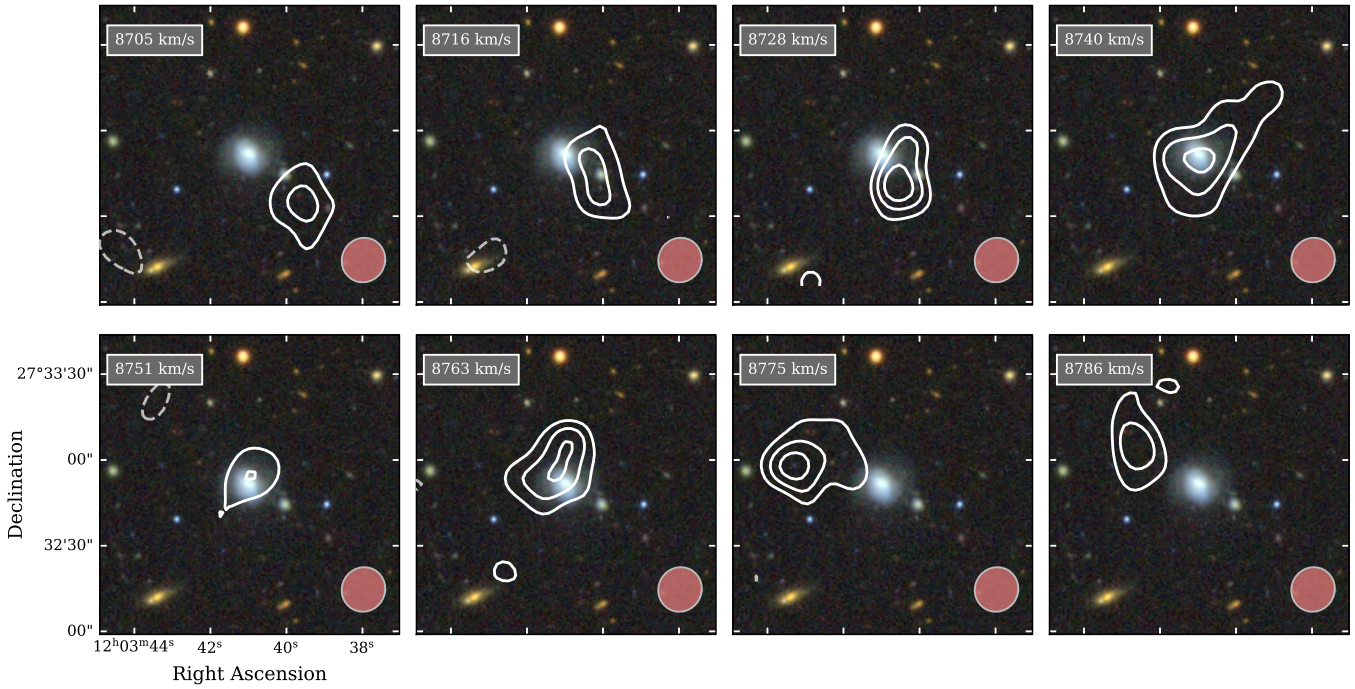

Figure 4. GMRT channel maps of the host of FRB 20181223C, overlaid on DECam imaging. Contours are at 1.0, 1.5, 2.0 mJy beam^{-1}, with dashed contours signifying negative counterparts.

of this elongation, we employ `3DBarolo` to fit a smooth rotation disk profile, and compare with the data (see Fig. 12 in Appendix), which verifies this emission is not standard for a settled galaxy. The flux level of these features is near the noise level, and thus they are not contributing significantly to the asymmetry metrics, though the A_{3D} result is not far from that of the disturbed host of FRB 20171020A. We also note that the DECam photometry hints at a potential perturbation to the stellar distribution on the north east side, with the spiral arm extending in a slightly unexpected direction to the north.

As the disturbance is spread across the entire northern face, and the velocity map shows no evidence of the more uniform bulk motion expected from a wind-driven outflow, this feature is most likely caused by a recent or ongoing minor tidal interaction. There are a number of nearby extended sources in the DECam imaging, though the only HI detection visible in MeerKAT arises from a large spiral 1.6 Mpc to the south. The tip of the outer contour in the 2532 km s^{-1} channel map, which shows the most extreme elongation, appears to overlap with a faint extended source, though this is likely a coincidence. Unfortunately, with no further redshift information on the surrounding objects, it is not possible to definitively characterise the system. Regardless, these HI observations reveal that NGC 4602 is another disturbed FRB host galaxy.

5.6 FRB 20210405I

The host of FRB 20210405I appears almostly perfectly symmetrical in the MeerKAT data. The `3DACs` code returned an A_{3D} value of -1, signifying no statistically significant asymmetry, and thus we conclude this host is undisturbed. According to the SoFiA-2 source finder, this galaxy is also isolated in HI.

5.7 FRB 20211127I

The host of FRB 20211127I was previously analysed in Glowacki et al. (2023) using low resolution ASKAP data, and was prior to this study the only non-interacting FRB host observed in HI. The detection appeared symmetric in spatial and spectral dimensions, but the authors concluded that higher resolution data would be required to fully confirm this case.

The new MeerKAT observation does indeed reveal a mostly symmetrical HI distribution, both in the spectra and intensity map. The 1D asymmetry measurements are the lowest in this study, and while A_{3D} value returned by `3DACs` is not -1, it is low. This is perhaps due to the slight elongation in the north east corner of the intensity map, but neither the channel nor velocity maps indicate anything definitive. Thus, we conclude that this host galaxy is undisturbed. Interestingly, it is worth noting that unlike the previous two undisturbed hosts, this galaxy is in a rich HI group. Three nearby galaxies are detected in this deeper MeerKAT observation, none of which were present in the WALLABY Pilot Survey II observation of this field (Glowacki et al. 2023). The nearest neighbour lies roughly 2.4 Mpc away.

5.8 FRB 20211212A

The faint emission from this high redshift host appears to be symmetrical, though neither the spectral nor spatial resolution is great enough to properly describe it. We conclude that it is mostly likely an undisturbed galaxy, but deeper observations

https://doi.org/10.1017/pasa.2025.10123 Published online by Cambridge University Press

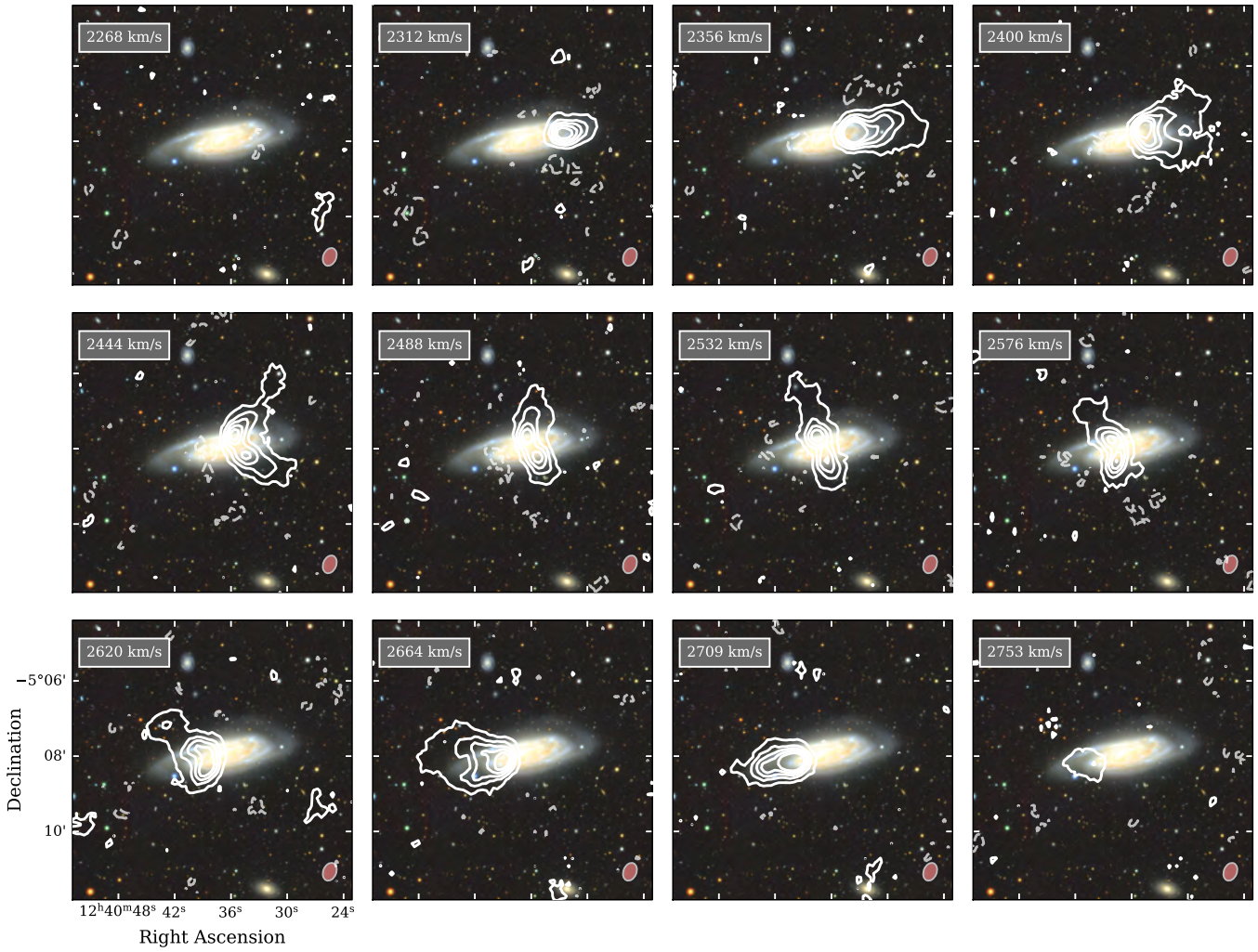

Figure 5. MeerKAT individual channel maps of the host of FRB 20200723B, overlaid on DECam imaging. Contours are at 1, 3, 5, 7, and 9 mJy beam^{-1}, with dashed contours signifying negative counterparts.

would be needed to confirm this. This host has two faint HI neighbours that each lie approximately 2 Mpc away.

5.9 FRB 20231229A

The host of FRB 20231229A is a face-on spiral that appears to have a significant disturbance to one of its spiral arms. The Arecibo spectrum shows a moderately asymmetric profile, resulting in an $A_{\rm flux}$ value above our threshold for asymmetry. We consider it likely that this target is disturbed, but interferometric observations are required to fully reveal the nature of this.

5.10 FRB 20231230A

As this target was detected in an off-centred observation, the noise level dominates its HI spectrum. It appears slightly asymmetric, but with such low resolution data, is not possible to accurately quantify, as shown by the enormous uncertainties in the asymmetry metrics. Targeted observations are required to ascertain the true nature of this host.

5.11 FRB 20240201A

The host of FRB 20240201A is an edge-on spiral galaxy in an apparent galaxy pair. Spectroscopic observations from the Sloan Digital Sky Survey (SDSS) reveal the two share similar redshifts; 0.04273 and 0.04314 for the host and neighbour respectively. The moment maps clearly show an overlap in the clouds surrounding the two galaxies. The data displayed was processed with a robust weighting of 0.5; a weighting of 2 reveals the extent of the combined gas cloud reaches far beyond the combined optical region, whilst a weighting of 0 is unable to pick up the emission of the FRB host.

The spectra presented in Fig. 1 show the superposition of both galaxies' emission. The host contributes partially to the first peak but is dominated by the neighbour; examining the resolved MeerKAT data reveals the neighbour's rotating arms form the bulk of the outer peaks and its notably gas rich central bulge forms the third peak in the centre. The slightly blueshifted nature of the HI emission originating from the position of the FRB host, seen in the MeerKAT moment 1 map, confirms that it is not simply emission from the edges of

https://doi.org/10.1017/pasa.2025.10123 Published online by Cambridge University Press

the neighbour's HI cloud.

Inspecting the SoFiA-2 mask confirms that there is a smooth emitting connection in both physical and spectral space between the two galaxies. From this, it is clear that the pair are tidally interacting, and likely have been for some time. A good amount of emission from the neighbour is arising from directly behind the host, and thus it is not possible to cleanly extract an HI spectra for it alone. As such, we calculate global properties for the pair as a whole, and do not attempt to measure the asymmetry metrics. This interaction observed in HI correlates with the apparent distortion of the stellar disk in the south west of the neighbouring galaxy towards the FRB host, as seen in the DECam imaging. The velocity dispersion map reveals heightened turbulence in the region between the two, highlighting the impact of their gravitational influences.

5.12 FRB 20240210A

The spiral host of FRB 20240210A lies only 1.5' from of a smaller neighbour to the south west, and both exhibit clear HI emission. When imaging with a Briggs weighting with a robust value of 2, SoFiA-2 considers the galaxies to be connected. However, the significance of any potential tidal bridge is extremely marginal; even when rebinned from a spectral resolution of 26 kHz to 104 and 208 kHz resolutions, the link never rises above 2σ, and is completely absent when imaging with a robust weighting of 0.5. Furthermore, individual channel maps do not suggest any consistent extension of the host galaxy.

Given the neighbour's archival redshift of 0.02360 from the 2dF Galaxy Redshift Survey (Colless et al. 2001), the angular separation deprojects into a physical distance of roughly 1 Mpc. The spectral profile of the host is symmetric, and none of the asymmetry metrics hint at intrinsic disruption. As such, we do not consider this host to be tidally interacting with the neighbour, and thus is undisturbed.

5.13 FRB 20240312D

The host of FRB 20240312D shows an unusual gas distribution in its intensity map, with the emission extending further to the south than to the north. Channel maps, presented in Fig. 6, confirm this asymmetry, as the southern extension is present across at least a third of the velocity profile. However, these features are less significant than in previous hosts: they do not reach the high contour levels seen in the host of FRB 20181223C, nor are they highly resolved by the beam as in the host of FRB 20200723B, making the evidence less conclusive. This is further reflected in the host's A_{3D} value of 0.199, which sits above every undisturbed host and below every disturbed host.

This galaxy resides in a highly rich HI group containing at least eight nearby HI galaxies, a number of which are within 1 Mpc. Cross-matching these detections with DECam imaging reveals that, apart from one case, they are all small, faint dwarf galaxies. The larger edge-on spiral visible to the south in Fig. 6 appears close in projection, but the central frequency of its strong HI line places it nearly 10 Mpc in the background. Consequently, the nearest companion to the FRB host lies roughly 600 kpc to the east. Given the host exists in such a dense environment, and the observed gas extension does not point toward the nearest neighbour, it is more likely that the asymmetry is simply a lingering imprint of an earlier gravitational perturbation caused during the formation of the group than a recent tidal interaction. In these cases, peripheral gas can take considerable time to resettle into the disk. We therefore regard this host as a middle-ground case and, in Section 6, examine it under both classifications when interpreting the results.

5.14 FRB 20240615B

The HI emission arising from this distant host appears largely symmetrical. The line is narrow, but the double-horned profile is still resolved, with the peaks reaching similar intensities. Neither its moment maps nor its asymmetry metrics suggest any disturbance, and thus we conclude this host is settled. It is worth noting that this galaxy does lie in a relatively HI rich group, with at least four galaxies within 10 Mpc, the nearest positioned roughly 900 kpc away.

5.15 FRB 20250316A

NGC 4141 is a slightly inclined spiral that shows a highly asymmetric line profile in the archival Effelsberg spectrum. In particular, its A_{flux} parameter is the highest robust measurement in this sample. PanSTARRS imaging reveals that a highly elongated uncatalogued galaxy lies very nearby; it appears very similar in colour profile to NGC 4141, and thus may well have a similar redshift. If this were to be the case, the two would almost certainly be interacting, which would likely be the cause of the profile asymmetry. Therefore, this region is a prime target for future interferometric observations to resolve its spatial HI distribution.

6. Discussion

6.1 Are FRB Hosts Disturbed?

From this analysis, we find that six of these FRB host galaxies are disturbed: FRB 20181223C, FRB 20190418A, FRB 20200723B, FRB 20231229A, FRB 20240201A, and FRB 20250316A. Another six are clearly undisturbed: FRB 20190425A, FRB 20210405I, FRB 20211127I, FRB 20211212A, FRB 202404210A, and FRB 20240615B. One is borderline (FRB 20240312D), and the remaining three require deeper/targeted observations to draw firm conclusions. With respect to the total population of FRB hosts now observed in HI the confirmed ratio of disturbed to undisturbed galaxies is 11:6.

Comparing this ratio to background populations is somewhat nebulous. While in Section 4.2 we quantify the thresholds for disturbance with respect to the asymmetry metrics, we have not relied solely on these values as indicators of disruption. In fact, at least two of the hosts we consider disturbed here may not have been considered so in large volume surveys. For example, determining the disrupted nature of the host of FRB 20200723B required in-depth analysis of individual channel maps at low flux thresholds; none of the asymmetry metrics

https://doi.org/10.1017/pasa.2025.10123 Published online by Cambridge University Press

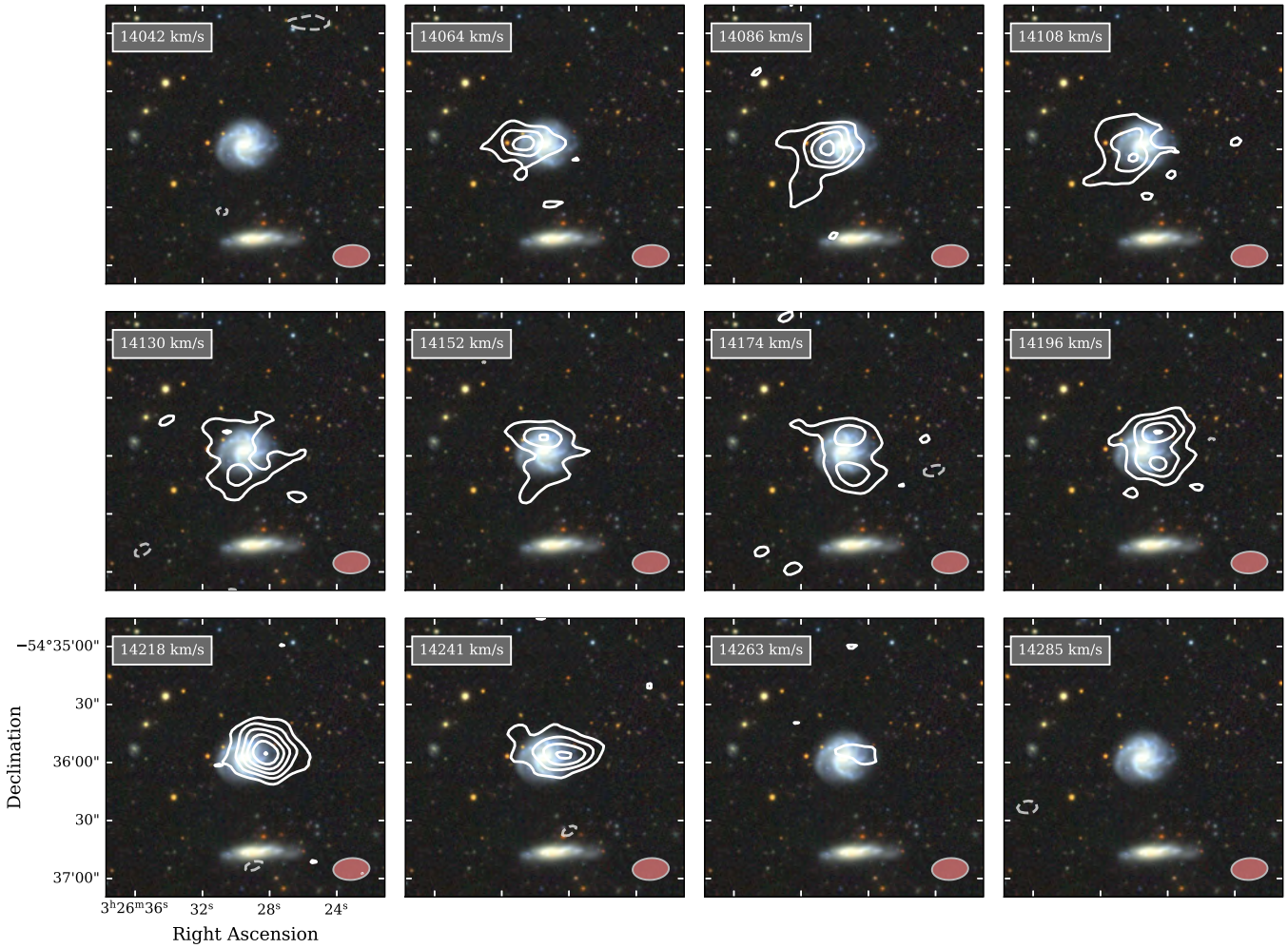

Figure 6. MeerKAT individual channel maps of the host of FRB 20240312D, overlaid on DECam imaging. Contours are at 0.4, 0.8, 1.2, 1.6, 2.0, and 2.4 mJy beam^{-1}, with dashed contours signifying negative counterparts.

would otherwise suggest this nature. It is likely that digging deep enough would reveal that the fraction of nearby galaxies with some low level disruption similar to this is much higher than the fractions reported from asymmetry quantification methods.

Therefore, the observation that ∼65% of FRB hosts are disturbed cannot be directly contrasted to the 10-40% results in the literature. In Figure 7, we do utilise the $A_{\rm flux}$ and $A_{\rm spec}$ metrics to compare with the LVHIS and HALOGAS samples as is done in Michalowski (2021) and Glowacki et al. (2024), and also include approximations for the xGASS (Catinella et al. 2018) and HIPASS (Barnes et al. 2001) datasets. These are stellar mass and HI mass selected samples that span a wide range of environments and masses, and thus are more representative of the local galaxy population. We estimate their $A_{\rm flux}$ values by extracting the data from Watts et al. (2020, Fig. 2) and Reynolds, Westmeier, and Staveley-Smith (2020, Table 5) respectively. We note that robust comparison should be done exclusively with galaxies similar in mass and SFR to FRB hosts; however, both Watts et al. 2020; Reynolds et al. 2020 find no evolution in $A_{\rm flux}$ or $A_{\rm spec}$ as a function of mass, and thus comparing with these samples is satisfactory. Our sample of FRB hosts exhibits slightly higher 1D asymmetry levels than the background galaxy population, though the discrepancy is minimal — particularly when compared to the more representative background samples.

As discussed in Section 4.2, comparing our $A_{\rm 1D}$, $A_{\rm 2D}$, and $A_{\rm 3D}$ values to literature is largely non-viable. Perron-Cormier et al. (2025) only includes figures of their $A_{\rm 1D}$ and $A_{\rm 3D}$ distributions for the ∼31% of galaxies in their sample which had $A_{\rm 3D} \geq 0$ (i.e. not -1). Thus, these results are inherently biased against settled galaxies.

All this considered, we cannot definitively claim what the disturbed-to-settled ratio for background galaxies is in a way that is meaningful for comparison with our sample. We speculate that it should hover somewhere near 1:1 considering the quantified asymmetry percentages of background galaxies and including some allowance for the more detailed analysis we have used to characterise our sample. Under this assumption, the observed rate of disturbance in FRB hosts remains higher than expected.

To quantitatively assess the significance of this, we can

https://doi.org/10.1017/pasa.2025.10123 Published online by Cambridge University Press

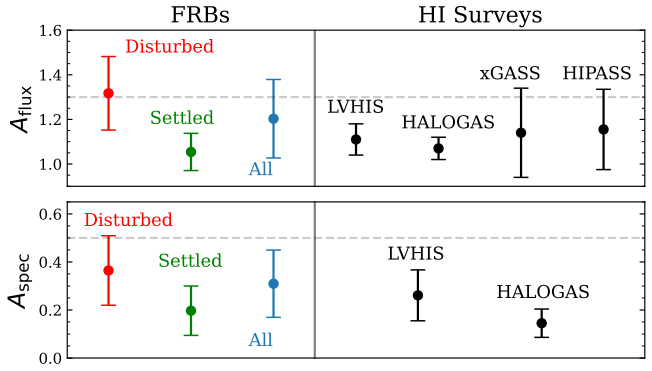

Figure 7. A_{flux} and A_{spec} values of FRB hosts compared to background populations presented in Reynolds et al. (2020) and Watts et al. (2020). LVHIS and HALOGAS sample low-density environments, whereas xGASS is more representative of the local galaxy population. The xGASS result is an approximation; we generate the results by extracting the cumulative distribution of Fig. 2 from Watts et al. (2020). The two dashed lines indicate our chosen thresholds for asymmetry, outlined in Sec. 4.2.

assume Poisson error, and perform a likelihood ratio test. If our null hypothesis is that the ratio should follow 1:1 — i.e. the Poisson λ variable for both the disturbed and undisturbed host galaxy counts is 8.5 in this case — then a result of 11:6 results in a p-value associated with rejecting this hypothesis of 0.222. This is far higher than the standard significance threshold of 0.05; even considering the borderline case of FRB 20240312D as a disturbed host only shifts the p-value to 0.153. As such, we find that the earlier apparent trend suggesting underlying disturbance in FRB host galaxies is no longer statistically significant. While our observations, which reveal that 21 of 22 FRB hosts emit in HI, further link FRB progenitors with star formation, the data provide no evidence that merger-induced star formation enhancement plays a significant role in their production.

6.2 HI Properties of FRB Hosts

As with most other galaxy population measurements, FRB hosts appear to span a broad range of values with respect to their global HI properties. In Figure 8, we compare our hosts with the xGASS dataset (Catinella et al. 2018) and with previously analysed FRB hosts. Hosts of non-repeaters are shown in red, and hosts of repeaters are shown in blue. All of our new FRBs are non-repeaters, other than FRB 20200223B, whose host is our only non-detection. Measurements of stellar mass and SFR in the xGASS sample are derived from UV and mid-IR observations, tracing the past 100 Myrs of star-formation history (SFH). The values we use for our FRB hosts are taken from SED fitting in the respective localisation papers (see Table 1). The hosts of FRB 20210405I, 20240312D, and 20240615B have not had SED fitting, and thus we derive stellar mass approximations using their 2MASS K-band magnitudes and the mass-luminosity relation for spiral galaxies (McGaugh and Schombert 2014), and use their RC-derived SFRs, which should probe similar timescales of SFH to SED fitting; these hosts are shown with unfilled stars in Fig. 8.

Panel (a) shows that FRB hosts have standard SFRs for their HI masses, but are mostly massive in HI ($M_{\rm HI} > 10^{9.5} M_\odot$) with respect to the background population, which aligns with the stellar mass trend observed in optical studies (Gordon et al. 2023; Sharma et al. 2024). Interestingly, the four repeater hosts appear to lie towards the less massive end of the FRB host HI mass range; Gordon et al. (2023) and Sharma et al. (2024) also noted a similar pattern in their stellar masses. However, due to the low number of repeaters in their samples (6 and 5), significance tests found no statistical evidence for such a trend. However, Chen et al. (2025) presented a comparison between $M_\star$ and SFR(Hα) in 11 repeater and 33 non-repeater hosts, and found a statistically significant separation (p-value of 0.0203 when excluding high redshift non-repeaters) between the two populations when considering both properties in tandem.

Only one of the repeater hosts in our sample was included in any of the stellar mass studies above, potentially providing further evidence to separate repeater and non-repeater host populations based on mass. However, with such a small number of targets, and given the level of overlap observed in panel (a), this phenomenon is clearly not yet significant. To verify this, we run a simple two sample Kolmogorov-Smirnov (KS) test on the HI masses of our sample, and also run a MANOVA (Multivariate Analysis of Variance) test (as in Chen et al. 2025) on the multivariate domain of $M_{\rm HI}$ vs. SFR. In each case, we find p-values greater than 0.05 (0.11 and 0.16 respectively). Regardless, future HI studies of FRB hosts should consider probing this relation a focus.

Panel (b) of Fig. 8 shows that the average gas fractions ($M_{\rm HI}/M_\star$) of FRB hosts are greater than background galaxies; because all of our hosts are spirals, this is expected. With respect to xGASS galaxies with HI detections (which are much more likely to be late-type galaxies), the FRB hosts are slightly gas-rich, but are spread widely about the median.

Panel (c) displays a more robust relationship between gas fraction and specific SFR (sSFR), used by Kaur, Kanekar, and Prochaska (2022) and Glowacki et al. (2023) to assess if any large gas mass had recently been deposited into the galaxy through a merger. FRB hosts tend to lie above the median for HI detected xGASS galaxies, but the spread again is quite large. The highly interacting host of FRB 20180916B (upper blue diamond) lies further above its respective bin median than any in our new sample; however, the two disturbed hosts presented in Michalowski (2021) fall below this median, demonstrating that this relationship is not necessarily a consistent indicator of overall disturbance.

We see no noticeable trend in any of these three plots when colour-coding by our disturbance assessment (see Fig. 13 in Appendix). We also see no significant difference between the disturbance in isolated galaxies vs. those in HI groups.

6.3 The Baryon Fraction of FRB Hosts

We briefly consider the baryon fractions, $(M_\star + M_{\rm HI})/M_{200}$, of FRB host galaxies (excluding the CGM). We reiterate that our estimates of M_{200} are not particularly robust due to the unconsidered errors in $V_{\rm rot}$ arising from inclination uncertainties and

https://doi.org/10.1017/pasa.2025.10123 Published online by Cambridge University Press

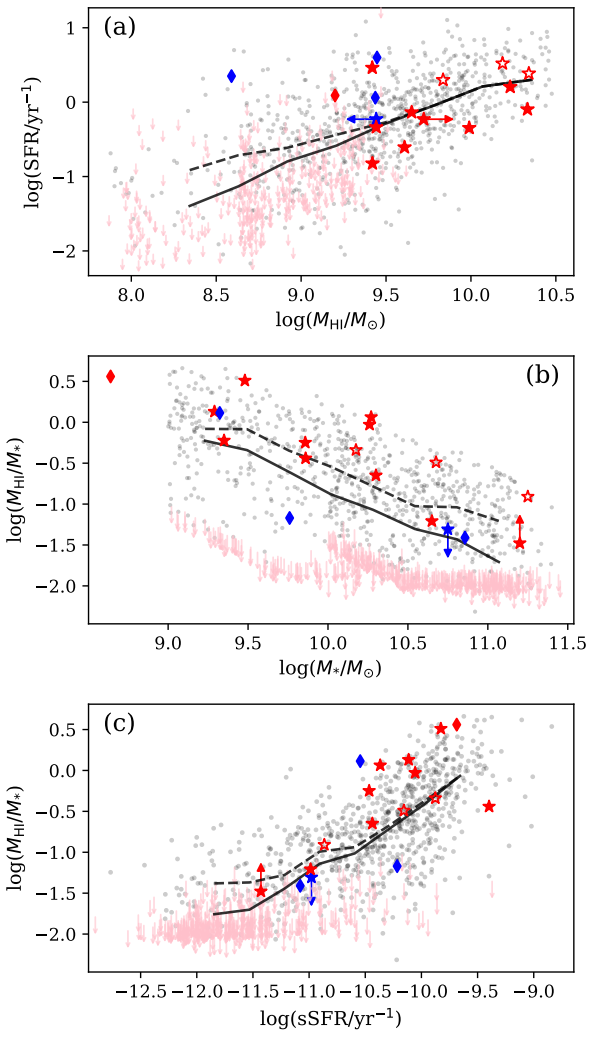

Figure 8. Global HI properties of FRB hosts, separated into non-repeating (red) and repeating (blue) FRBs. Stars indicate our sample, and diamonds indicate the previously published hosts. These are overlaid on the xGASS sample (grey = detected in HI, pink = non-detections in HI) (Catinella et al. 2018). The FRB host stellar masses and SFRs are taken from literature SED modelling values where possible; open stars represent hosts without SED fitting, where we derive M_* from literature K-band luminosities and use our radio continuum SFR estimates (see Table 3). The black lines indicate the median values at eight arbitrary bins along the x-axis for all xGASS galaxies (solid line) and for just HI detected galaxies (dashed line).

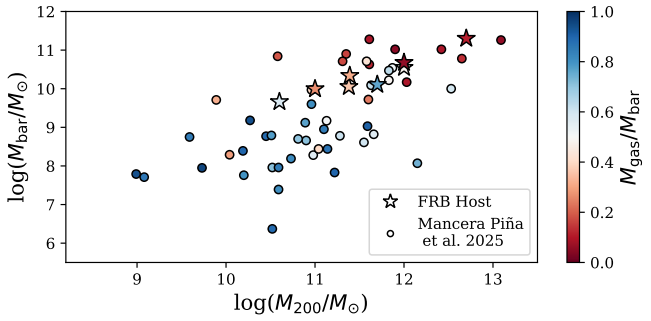

Figure 9. Baryonic vs. virial masses for FRB hosts and the sample of Mancera Piña et al. (2025).

instrumental effects. Figure 9 compares the galaxy baryonic mass M_{bar}=$M_\star$ + M_{HI} with M_{200} for our selection of hosts and a recent background sample of galaxies from Mancera Piña et al. (2025). It is clear that these FRB hosts are typical when considering this relation, falling generally in line with the background sample in both spatial distribution and gas-baryon fraction, which is indicated by colour. The scatter in this relation is wide, and thus even our rough estimates for M_{200} allow this conclusion to be drawn.

6.4 Connecting HI Observations with the DM of FRB Hosts

In addition to using HI to probe the properties of FRB hosts beyond the stellar disk, such observations can be broadly utilised as a proxy for electron column density. Disentangling the host galaxy contribution from the measured dispersion measure (DM) is a pressing issue for cosmological studies using FRBs (for a review, see Glowacki and Lee 2025). The free electrons which contribute to the DM arise from the ionised hydrogen (HII) gas; assuming standard ionisation fractions, HII column densities can be derived from HI column densities. As such, highly resolved HI maps could theoretically be used to better pin down the contribution of the host to the DM.

Local Universe FRBs are particularly useful for this approach. Any uncertainty in the excess DM of an FRB - the remaining contribution when subtracting the Milky Way's disk and halo contributions and the median intergalactic medium contribution as predicted by the Macquart relation (Macquart et al. 2020) — will not be dominated by the scatter on the Macquart relation, and instead will encode information about errors in the estimations of the Milky Way ISM and halo contributions. Recording the HI surface density at the location of an FRB thus may offer clues as to the expected density of free electrons along the line of sight in the host galaxy. Of course, a number of drawbacks — e.g. the lack of knowledge about the projected distance of the progenitor inside the host, and the quality of the assumptions made regarding ionisation fractions — limit the efficacy of this approach. However, given the lack of alternative prior information constraining the DM contribution of the host, this is a valid avenue to investigate.

Unfortunately, the maps presented in this study are unlikely to provide significant constraints; the majority of these FRBs are not localised to high enough precision, and the beam sizes likely preclude the measured column densities from being accurately representative of the line of sight to the FRB. As such, we do not attempt a correlation between excess DM and our derived HI properties, leaving this for future work with a larger, well-localised sample.

6.5 3D Asymmetry Quantification

Having utilised `3DACs` to measure 3D asymmetry in these host galaxies, we can assess the considerations that are likely to be important for future studies which do the same. Of course, we reiterate that only three of these targets satisfy the spatial resolution requirements outlined in Deg et al. (2020) for robust asymmetry modelling. However, using just these

https://doi.org/10.1017/pasa.2025.10123 Published online by Cambridge University Press

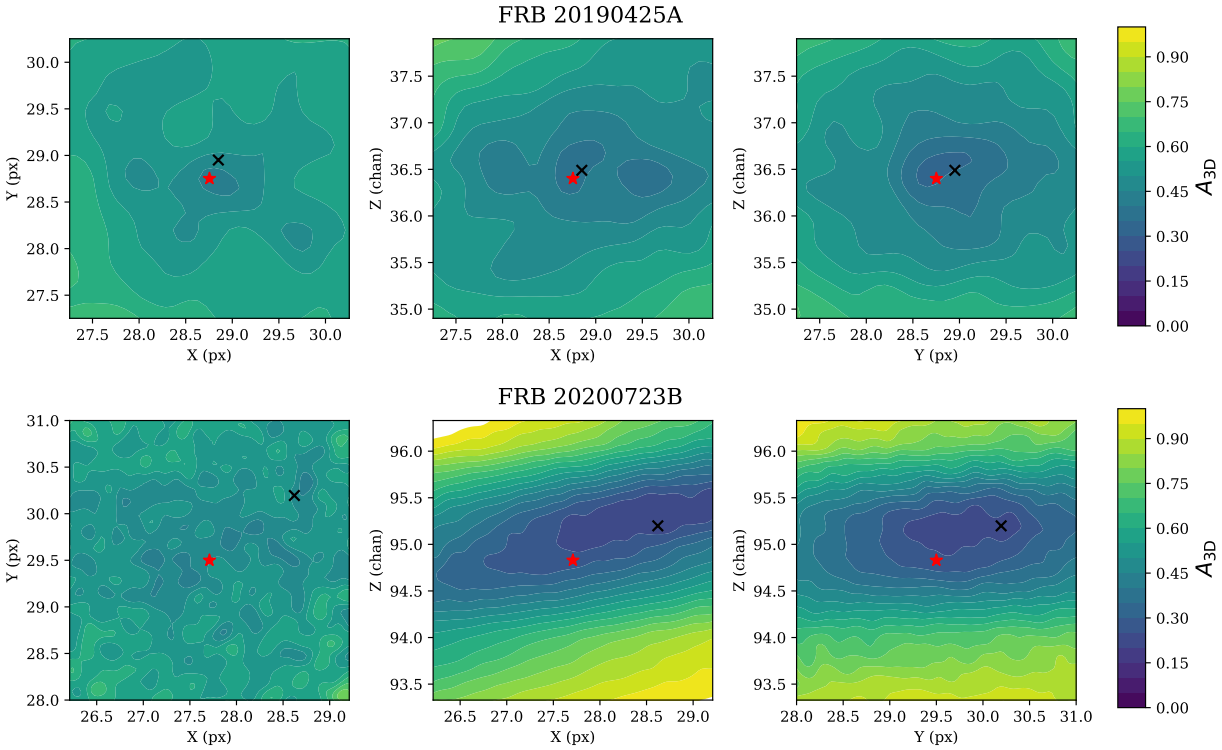

Figure 10. Smoothed sampling of the A_{3D} volumes for the hosts of FRB 20190425A and FRB 20200723B, which both pass the resolution requirements for robust A_{3D} measurement according to Deg et al. (2023). The red star in the centres show the location of the fractional 3D voxel used for our measurements, and the black crosses designate the location of the flux-weighted centre. The slightly disturbed host of FRB 20200723B shows a much greater discrepancy between the two points, which corresponds to a significantly different measured value of A_{3D}.

we can clearly show how difficult it can be to make physically meaningful asymmetry measurements.

Figure 10 presents a smoothed sampling of the A_{3D} space with respect to the choice of central (x,y,z) voxel, for the hosts of FRB 20190425A and FRB 20200723B. The red stars represent the chosen rotation centre (i.e. the flux-weighted spectral centre of the optical centre of brightness) whereas the black crosses represent simply the flux-weighted centre of the masked cube. It can be seen that very slight changes in the choice of rotation voxel can lead to significant variations in the returned A_{3D} value.

The host of FRB 20190425A is undisturbed, and thus the discrepancy between the A_{3D} value measured using our chosen centre and the flux-weighted centre is just 0.009. However for the slightly disturbed host of FRB 20200723B, using the latter cuts the measured value in half, from 0.210 to 0.108 This makes intuitive physical sense; a flux-weighted centre will always be biased by extended/disrupted emission. However, it is interesting to observe how significantly this impacts the asymmetry quantification even for such a low level disruption, essentially completely concealing its existence. Thus, we recommend that if kinematic modelling is not possible/feasible in order to ascertain a kinematic centre, it is certainly worth deriving the rotation voxel from optical data rather than HI data.

7. Conclusions

In this study, we have probed the HI emission from 17 FRB host galaxies to investigate the emerging trend of disturbance and asymmetry in the population. We detect emission from 16 of these; the other is known to be transitioning to a quiescent stage and thus is less likely to contain a significant gas reservoir. By examining the spectra and intensity maps, and using various asymmetry quantification metrics, we identify six hosts which are disturbed, four which are not, and three which require deeper observations to draw clear conclusions on. Incorporating past results leads to a disturbed-to-settled HI profile ratio for FRB hosts of 11:6, which tells a much different story to the previous ratio of 5:0 (or 5:1 when including the inconclusive result of Glowacki et al. 2023). The ratio we find yields a p-value of 0.222 under the assumption of an underlying 1:1 distribution as is roughly expected of the background galaxy population. This clearly signifies that the observed excess of disturbance in FRB hosts is not statistically significant, dispelling any consistent underlying link between FRB progenitor formation and host galaxy merger activity. However, given 21 of 22 FRB hosts now observed in HI do indeed contain emitting HI reservoirs, the connection between these progenitors and star formation is further solidified.

In accordance with their optically derived stellar masses, FRB host galaxies are mostly massive in HI, but exhibit a spread in gas and baryon fraction that is unremarkable with respect to the background population. Hosts of repeating FRBs may

https://doi.org/10.1017/pasa.2025.10123 Published online by Cambridge University Press

be slightly less massive on average than those of apparently non-repeating FRBs, though our sample size is too small to draw firm conclusions. Similar observations have been noted in recent stellar-mass studies, but significance tests in those works fail to confirm a difference; we perform comparable tests on our independent sample of repeater hosts and likewise find no statistically significant difference.

With a number of low-z FRBs localised since the start of this study, and with CHIME DR2 on the horizon, a significantly larger sample of local Universe FRB hosts should be observable in HI in the near future. Highly resolved HI maps of these hosts may offer clues to aid in disentangling their contributions from the measured DM of FRBs. Future works with a large sample of arcsecond localised nearby FRBs should aim to investigate the relation between HI column density and excess DM, and should also focus on probing the potential mass discrepancy between the hosts of repeating and non-repeating FRBs.

Acknowledgement

We thank Ron Ekers and Kristine Spekkens for useful discussions, and Lucia Marchetti for providing access to a dataset analysed in this work. H.R. is supported by an Australian Government Research Training Program (RTP) Scholarship. M.G. and C.W.J. acknowledge support by the Australian Government through the Australian Research Council Discovery Projects funding scheme (project DP210102103). M.G. also acknowledges support through UK STFC Grant ST/Y001117/1. For the purpose of open access, the author has applied a Creative Commons Attribution (CC BY) licence to any Author Accepted Manuscript version arising from this submission. M.C. acknowledges support from the Australian Research Council Discovery Early Career Research Award (project number DE220100819). A.C.G. and the Fong Group at Northwestern acknowledges support by the National Science Foundation under grant Nos. AST-1909358, AST-2308182 and CAREER grant No. AST-2047919. J.X.P., A.C.G. acknowledge support from NSF grants AST-1911140, AST-1910471 and AST-2206490 as members of the Fast and Fortunate for FRB Follow-up team. ATD acknowledges support through Australian Research Council Discovery Project DP22010230.

This scientific work uses data obtained from Inyarrimanha Ilgari Bundara, the CSIRO Murchison Radio-astronomy Observatory. We acknowledge the Wajarri Yamaji People as the Traditional Owners and native title holders of the Observatory site. CSIRO's ASKAP radio telescope is part of the Australia Telescope National Facility (https://ror.org/05qajvd42). Operation of ASKAP is funded by the Australian Government with support from the National Collaborative Research Infrastructure Strategy. ASKAP uses the resources of the Pawsey Supercomputing Research Centre. Establishment of ASKAP, Inyarrimanha Ilgari Bundara, the CSIRO Murchison Radio-astronomy Observatory, and the Pawsey Supercomputing Research Centre are initiatives of the Australian Government, with support from the Government of Western Australia and the Science and Industry Endowment Fund. We also thank the MRO site staff. The MeerKAT telescope is operated by the South African Radio Astronomy Observatory, which is a facility of the National Research Foundation, an agency of the Department of Science, Technology and Innovation.

We acknowledge the use of the ilifu cloud computing facility—www.ilifu.ac.za, a partnership between the University of Cape Town, the University of the Western Cape, Stellenbosch University, Sol Plaatje University, the Cape Peninsula University of Technology, and the South African Radio Astronomy Observatory. The ilifu facility is supported by contributions from the Inter- University Institute for Data Intensive Astronomy (IDIA—a partnership between the University of Cape Town, the University of Pretoria, and the University of the Western Cape), the Computational Biology division at UCT, and the Data Intensive Research Initiative of South Africa (DIRISA). This work was carried out using the data processing pipelines developed at the Inter-University Institute for Data Intensive Astronomy (IDIA) and available at https://idia-pipelines.github.io. IDIA is a partnership of the University of Cape Town, the University of Pretoria, and the University of the Western Cape. This work made use of the CARTA (Cube Analysis and Rendering Tool for Astronomy) software (https://cartavis.github.io; Comrie et al. 2021), and the iDaVIE (immersive Data Visualisation Interactive Explorer) software (https://idavie.readthedocs.io/en/latest/; Marchetti et al. 2022) This research has made use of the NASA/IPAC Extragalactic Database (NED), which is operated by the Jet Propulsion Laboratory, California Institute of Technology, under contract with the National Aeronautics and Space Administration.

References

Adams, E. A.K., B. Adebahr, W. J.G. De Blok, H. Dénes, K. M. Hess, J. M. Van Der Hulst, A. Kutkin, et al. 2022. First release of Apertif imaging survey data. *Astronomy and Astrophysics* 667:1–19. ISSN: 14320746. https://doi.org/10.1051/0004-6361/202244007. arXiv: 2208.05348.

Aggarwal, Kshitij, Tamás Budavári, Adam T. Deller, Tarraneh Eftekhari, Clancy W. James, J. Xavier Prochaska, and Shriharsh P. Tendulkar. 2021. Probabilistic association of transients to their hosts (path). *The Astrophysical Journal* 911 (2): 95. ISSN: 0004-637X. https://doi.org/10.3847/1538-4357/abe8d2. arXiv: 2102.10627. http://dx.doi.org/10.3847/1538-4357/abe8d2.

Alonso, M. Sol, Patricia B. Tissera, Georgina Coldwell, and Diego G. Lambas. 2004. Galaxy pairs in the 2df survey - ii. effects of interactions on star formation in groups and clusters. *Monthly Notices of the Royal Astronomical Society* 352 (3): 1081–1088. ISSN: 00358711. https://doi.org/10.1111/j.1365-2966.2004.08002.x. arXiv: 0401455 [astro-ph].

Bandura, Kevin, Graeme E. Addison, Mandana Amiri, J. Richard Bond, Duncan Campbell-Wilson, Liam Connor, Jean-François Cliche, et al. 2014. Canadian Hydrogen Intensity Mapping Experiment (CHIME) pathfinder. In *Ground-based and airborne telescopes v,* edited by Larry M. Stepp, Roberto Gilmozzi, and Helen J. Hall, 9145:914522. Society of Photo-Optical Instrumentation Engineers (SPIE) Conference Series. July. https://doi.org/10.1117/12.2054950. arXiv: 1406.2288 [astro-ph.IM].

Bannister, K. W., A. T. Deller, C. Phillips, J. P. Macquart, J. X. Prochaska, N. Tejos, S. D. Ryder, et al. 2019. A single fast radio burst localized to a massive galaxy at cosmological distance. *Science* 365, no. 6453 (August): 565–570. ISSN: 10959203. https://doi.org/10.1126/science.aaw5903. arXiv: 1906.11476.

Barnes, D. G., L. Staveley-Smith, W. J.G. De Blok, T. Oosterloo, I. M. Stewart, A. E. Wright, G. D. Banks, et al. 2001. The HI Parkes All Sky Survey: Southern observations, calibration and robust imaging. *Monthly Notices of the Royal Astronomical Society* 322 (3): 486–498. ISSN: 00358711. https://doi.org/10.1046/j.1365-8711.2001.04102.x.

Bezuidenhout, M C, E Barr, M Caleb, L N Driessen, F Jankowski, M Kramer, M Malenta, et al. 2022. Meertrap : 12 galactic fast transients detected in a real-time , commensal meerkat survey. 1498:1483–1498.

Bhandari, Shivani, Kasper E. Heintz, Kshitij Aggarwal, Lachlan Marnoch, Cherie K. Day, Jessica Sydnor, Sarah Burke-Spolaor, et al. 2022. Characterizing the fast radio burst host galaxy population and its connection to transients in the local and extragalactic universe. *The Astronomical Journal* 163 (2): 69. ISSN: 0004-6256. https://doi.org/10.3847/1538-3881/ac3aec.

Bhardwaj, Mohit, Daniele Michilli, Aida Yu. Kirichenko, Obinna Modilim, Kaitlyn Shin, Victoria M. Kaspi, Bridget C. Andersen, et al. 2024. Host galaxies for four nearby chime/frb sources and the local universe frb host galaxy population. *The Astrophysical Journal Letters* 971 (2): L51. ISSN: 2041-8205. https://doi.org/10.3847/2041-8213/ad64d1. arXiv: 2310.10018.

Bochenek, C. D., V. Ravi, K. V. Belov, G. Hallinan, J. Kocz, S. R. Kulkarni, and D. L. McKenna. 2020. A fast radio burst associated with a galactic magnetar. *Nature* 587 (7832): 59–62. ISSN: 14764687. https://doi.org/10.1038/s41586-020-2872-x. arXiv: 2005.10828. http://dx.doi.org/10.1038/s41586-020-2872-x.

Bok, J., S. L. Blyth, D. G. Gilbank, and E. C. Elson. 2019. Enhanced h i profile asymmetries in close galaxy pairs. *Monthly Notices of the Royal Astronomical Society* 484 (1): 582–594. ISSN: 13652966. https://doi.org/10.1093/mnras/sty3448. arXiv: 1907.09877.

Catinella, Barbara, Amelie Saintonge, Steven Janowiecki, Luca Cortese, Romeel Davé, Jenna J. Lemonias, Andrew P. Cooper, et al. 2018. xGASS: Total cold gas scaling relations and molecular-to-atomic gas ratios of galaxies in the local Universe. *Monthly Notices of the Royal Astronomical Society* 476 (1): 875–895. ISSN: 13652966. https://doi.org/10.1093/mnras/sty089. arXiv: 1802.02373.

Chambers, K. C., E. A. Magnier, N. Metcalfe, H. A. Flewelling, M. E. Huber, C. Z. Waters, L. Denneau, et al. 2016. The Pan-STARRS1 Surveys. *arXiv e-prints* (December): arXiv:1612.05560. https://doi.org/10.48550/arXiv.1612.05560. arXiv: 1612.05560 [astro-ph.IM].

Chatterjee, S., C. J. Law, R. S. Wharton, S. Burke-Spolaor, J. W.T. Hessels, G. C. Bower, J. M. Cordes, et al. 2017. A direct localization of a fast radio burst and its host. *Nature* 541 (7635): 58–61. ISSN: 14764687. https://doi.org/10.1038/nature20797.

Chen, Xiang-Lei, Chao-Wei Tsai, Di Li, Pei Wang, Yi Feng, Jun-Shuo Zhang, Guo-Dong Li, et al. 2025. The Host Galaxy of the Hyperactive Repeating FRB 20240114A: Behind a Galaxy Cluster. *The Astrophysical Journal Letters,* no. Dm, arXiv: 2502.05587. http://arxiv.org/abs/2502.05587.

CHIME/FRB Collaboration, Mandana Amiri, Daniel Amouyal, Bridget C Andersen, Shion Andrew, Kevin Bandura, Mohit Bhardwaj, et al. 2025. A catalog of local universe fast radio bursts from chime/frb and the kko outrigger, arXiv: 2502.11217. http://arxiv.org/abs/2502.11217.

CHIME/FRB Collaboration, Mandana Amiri, Bridget C. Andersen, Kevin Bandura, Sabrina Berger, Mohit Bhardwaj, Michelle M. Boyce, et al. 2021. The first chime/frb fast radio burst catalog. *The Astrophysical Journal Supplement Series* 257 (2): 59. ISSN: 0067-0049. https://doi.org/10.3847/1538-4365/ac33ab. arXiv: 2106.04352.

CHIME/FRB Collaboration, B. C. Andersen, K. M. Bandura, M. Bhardwaj, A. Bij, M. M. Boyce, P. J. Boyle, et al. 2020. A bright millisecond-duration radio burst from a galactic magnetar. *Nature* 587 (7832): 54–58. ISSN: 14764687. https://doi.org/10.1038/s41586-020-2863-y. arXiv: 2005.10324.

Chung, Aeree, J. H. van Gorkom, Jeffrey D. P. Kenney, Hugh Crowl, and Bernd Vollmer. 2009. VLA Imaging of Virgo Spirals in Atomic Gas (VIVA). I. The Atlas and the H I Properties. *Astrophysical Journal* 138, no. 6 (December): 1741–1816. https://doi.org/10.1088/0004-6256/138/6/1741.

Colless, Matthew, Gavin Dalton, Steve Maddox, Will Sutherland, Peder Norberg, Shaun Cole, Joss Bland-Hawthorn, et al. 2001. The 2dF Galaxy Redshift Survey: spectra and redshifts. 328, no. 4 (December): 1039–1063. https://doi.org/10.1046/j.1365-8711.2001.04902.x. arXiv: astro-ph/0106498 [astro-ph].

Connor, Liam, Vikram Ravi, Kritti Sharma, Stella Koch Ocker, Jakob Faber, Gregg Hallinan, Charlie Harnach, et al. 2025. A gas rich cosmic web revealed by partitioning the missing baryons. *Nature Astronomy* (April). ISSN: 23973366. https://doi.org/10.1038/s41550-025-02566-y. http://arxiv.org/abs/2409.16952.

Darg, D. W., S. Kaviraj, C. J. Lintott, K. Schawinski, M. Sarzi, S. Bamford, J. Silk, et al. 2010. Galaxy zoo: the properties of merging galaxies in the nearby universe - local environments, colours, masses, star formation rates and agn activity. *Monthly Notices of the Royal Astronomical Society* 401 (3): 1552–1563. ISSN: 13652966. https://doi.org/10.1111/j.1365-2966.2009.15786.x. arXiv: 0903.5057.

Deg, N., S. L. Blyth, N. Hank, S. Kruger, and C. Carignan. 2020. Systematically asymmetric: A comparison of H I profile asymmetries in real and simulated galaxies. *Monthly Notices of the Royal Astronomical Society* 495 (2): 1984–2001. ISSN: 13652966. https://doi.org/10.1093/mnras/staa1368. arXiv: 2005.06453.

Deg, N., M. Perron-Cormier, K. Spekkens, M. Glowacki, S. L. Blyth, and N. Hank. 2023. Measuring galaxy asymmetries in 3D. *Monthly Notices of the Royal Astronomical Society* 523, no. 3 (August): 4340–4352. ISSN: 13652966. https://doi.org/10.1093/mnras/stad1693. arXiv: 2306.02839.

Dey, Arjun, David J. Schlegel, Dustin Lang, Robert Blum, Kaylan Burleigh, Xiaohui Fan, Joseph R. Findlay, et al. 2019. Overview of the DESI Legacy Imaging Surveys. *The Astronomical Journal* 157 (5): 168. ISSN: 0004-6256. https://doi.org/10.3847/1538-3881/ab089d. arXiv: 1804.08657.

Driessen, L N, E D Barr, D A H Buckley, M Caleb, H Chen, W Chen, M Gromadzki, et al. 2024a. Frb 20210405i : a nearby fast radio burst localized to sub-arcsecond precision with meerkat. *Monthly Notices of the Royal Astronomical Society* 3673 (v): 3659–3673. https://doi.org/10.1093/mnras/stad3329.

———. 2024b. Frb 20210405i : a nearby fast radio burst localized to sub-arcsecond precision with meerkat. 3673 (v): 3659–3673.

Eftekhari, T., Y. Dong, W. Fong, V. Shah, S. Simha, B. C. Andersen, S. Andrew, et al. 2025. The massive and quiescent elliptical host galaxy of the repeating fast radio burst frb 20240209a. *The Astrophysical Journal Letters* 979 (2): L22. ISSN: 2041-8205. https://doi.org/10.3847/2041-8213/ad9de2.

Espada, D., L. Verdes-Montenegro, W. K. Huchtmeier, J. Sulentic, S. Verley, S. Leon, and J. Sabater. 2011. The amiga sample of isolated galaxies: viii. the rate of asymmetric h i profiles in spiral galaxies. *Astronomy and Astrophysics* 532:1–14. ISSN: 00046361. https://doi.org/10.1051/0004-6361/201016117.

Glowacki, M., A. Bera, K. Lee-Waddell, A. T. Deller, T. Dial, K. Gourdji, S. Simha, et al. 2024. H i, frb, what's your z: the first frb host galaxy redshift from radio observations. *The Astrophysical Journal Letters* 962 (1): L13. ISSN: 2041-8205. https://doi.org/10.3847/2041-8213/ad1f62.

Glowacki, M., K. Lee-Waddell, A. T. Deller, N. Deg, A. C. Gordon, J. A. Grundy, L. Marnoch, et al. 2023. Wallaby pilot survey: h i in the host galaxy of a fast radio burst. *The Astrophysical Journal* 949 (1): 25. ISSN: 0004-637X. https://doi.org/10.3847/1538-4357/acc1e3.

Glowacki, Marcin, and Khee-Gan Lee. 2025. Cosmology with fast radio bursts (January). http://arxiv.org/abs/2410.24072.

https://doi.org/10.1017/pasa.2025.10123 Published online by Cambridge University Press

Gordon, Alexa C., Wen-fai Fong, Adam T. Deller, Lachlan Marnoch, Sung-soon Lim, Eric W. Peng, Keith W. Bannister, et al. 2025. Mapping the spatial distribution of fast radio bursts within their host galaxies. *arXiv e-prints* (June). http://arxiv.org/abs/2506.06453.

Gordon, Alexa C., Wen-fai Fong, Charles D. Kilpatrick, Tarraneh Eftekhari, Joel Leja, J. Xavier Prochaska, Anya E. Nugent, et al. 2023. The demographics, stellar populations, and star formation histories of fast radio burst host galaxies: implications for the progenitors (February). http://arxiv.org/abs/2302.05465.

Gupta, Y., B. Ajithkumar, H. S. Kale, S. Nayak, S. Sabhapathy, S. Sureshkumar, R. V. Swami, et al. 2017. The upgraded GMRT: opening new windows on the radio Universe. *Current Science* 113, no. 4 (August): 707–714. https://doi.org/10.18520/cs/v113/i04/707-714.

Haynes, Martha P., Riccardo Giovanelli, Pierre Chamaraux, Luiz N. da Costa, Wolfram Freudling, John J. Salzer, and Gary Wegner. 1999. The [ITAL]I[/ITAL]-Band Tully-Fisher Relation for S[CLC]c[/CLC] Galaxies: 21 Centimeter H [CSC]i[/CSC] Line Data. *The Astronomical Journal* 117 (5): 2039–2051. ISSN: 00046256. https://doi.org/10.1086/300851.

Haynes, Martha P., Riccardo Giovanelli, Brian R. Kent, Elizabeth A. K. Adams, Thomas J. Balonek, David W. Craig, Derek Fertig, et al. 2018. The arecibo legacy fast alfa survey: the alfalfa extragalactic h i source catalog. *The Astrophysical Journal* 861 (1): 49. ISSN: 0004-637X. https://doi.org/10.3847/1538-4357/aac956. arXiv: 1805.11499. http://dx.doi.org/10.3847/1538-4357/aac956.

Haynes, Martha P., David E. Hogg, Ronald J. Maddalena, Morton S. Roberts, and Liese van Zee. 1998. Asymmetry in High-Precision Global H [CSC]i[/CSC] Profiles of Isolated Spiral Galaxies. *The Astronomical Journal* 115 (1): 62–79. ISSN: 00046256. https://doi.org/10.1086/300166.

Heald, G., G. Józsa, P. Serra, L. Zschaechner, R. Rand, F. Fraternali, T. Oosterloo, R. Walterbos, E. Jütte, and G. Gentile. 2011. The Westerbork Hydrogen Accretion in LOcal GAlaxieS (HALOGAS) survey. I. Survey description and pilot observations. *Astronomy and Astrophysics* 526 (February): A118. https://doi.org/10.1051/0004-6361/201015938. arXiv: 1012.0816 [astro-ph.CO].

Heintz, Kasper E., J. Xavier Prochaska, Sunil Simha, Emma Platts, Wen-fai Fong, Nicolas Tejos, Stuart D. Ryder, et al. 2020. Host galaxy properties and offset distributions of fast radio bursts: implications for their progenitors. *The Astrophysical Journal* 903 (2): 152. ISSN: 0004-637X. https://doi.org/10.3847/1538-4357/abb6fb.

Holwerda, B. W., N. Pirzkal, W. J.G. de Blok, A. Bouchard, S. L. Blyth, K. J. van der Heyden, and E. C. Elson. 2011. Quantified hi morphology - ii. lopsidedness and interaction in whisp column density maps. *Monthly Notices of the Royal Astronomical Society* 416 (4): 2415–2425. ISSN: 13652966. https://doi.org/10.1111/j.1365-2966.2011.17683.x. arXiv: 1104.3292.

Hotan, A. W., J. D. Bunton, A. P. Chippendale, M. Whiting, J. Tuthill, V. A. Moss, D. McConnell, et al. 2021. Australian square kilometre array pathfinder: i. system description. *Publications of the Astronomical Society of Australia* 38:1–31. ISSN: 14486083. https://doi.org/10.1017/pasa.2021.1. arXiv: 2102.01870.

Ibik, Adaeze L., Maria R. Drout, B. M. Gaensler, Paul Scholz, Daniele Michilli, Mohit Bhardwaj, Victoria M. Kaspi, et al. 2023. Proposed host galaxies of repeating fast radio burst sources detected by chime/frb (April). arXiv: 2304.02638. http://arxiv.org/abs/2304.02638.

James, C. W., E. M. Ghosh, J. X. Prochaska, K. W. Bannister, S. Bhandari, C. K. Day, A. T. Deller, et al. 2022. A measurement of hubble's constant using fast radio bursts. *Monthly Notices of the Royal Astronomical Society* 516, no. 4 (November): 4862–4881. ISSN: 13652966. https://doi.org/10.1093/mnras/stac2524. arXiv: 2208.00819.

Jing, Yingjie, Jie Wang, Chen Xu, Ziming Liu, Qingze Chen, Tiantian Liang, Jinlong Xu, et al. 2023. Hifast : an h i data calibration and imaging pipeline for fast, arXiv: arXiv:2401.17364v1.

Jonas, Justin L, and The MeerKAT Team. 2016. The meerkat radio telescope pos(meerkat2016)001. *Proceedings of Science,* 1–23. http://pos.sissa.it/.

Kaur, Balpreet, Nissim Kanekar, and J. Xavier Prochaska. 2022. A fast radio burst progenitor born in a galaxy merger. *The Astrophysical Journal Letters* 925 (2): L20. ISSN: 2041-8205. https://doi.org/10.3847/2041-8213/ac4ca8.

Kirsten, F., B. Marcote, K. Nimmo, J. W.T. Hessels, M. Bhardwaj, S. P. Tendulkar, A. Keimpema, et al. 2022. A repeating fast radio burst source in a globular cluster. *Nature* 602 (7898): 585–589. ISSN: 14764687. https://doi.org/10.1038/s41586-021-04354-w. arXiv: 2105.11445.

Kocz, J., V. Ravi, M. Catha, L. D'Addario, G. Hallinan, R. Hobbs, S. Kulkarni, et al. 2019. Dsa-10: a prototype array for localizing fast radio bursts. *Monthly Notices of the Royal Astronomical Society* 489 (1): 919–927. ISSN: 13652966. https://doi.org/10.1093/mnras/stz2219. arXiv: 1906.08699.

Koribalski, Barbel S., Jing Wang, P. Kamphuis, T. Westmeier, L. Staveley-Smith, S. H. Oh, A. R. López-Sánchez, et al. 2018. The local volume hi survey (lvhis). *Monthly Notices of the Royal Astronomical Society* 478 (2): 1611–1648. ISSN: 13652966. https://doi.org/10.1093/mnras/sty479.

Koribalski, Bärbel S., L. Staveley-Smith, T. Westmeier, P. Serra, K. Spekkens, O. I. Wong, K. Lee-Waddell, et al. 2020. WALLABY – an SKA Pathfinder H i survey. *Astrophysics and Space Science* 365 (7). ISSN: 1572946X. https://doi.org/10.1007/s10509-020-03831-4. arXiv: 2002.07311.

Lee-Waddell, Karen, Clancy W. James, Stuart D. Ryder, Elizabeth K. Mahony, Arash Bahramian, Barbel S. Koribalski, Pravir Kumar, et al. 2023. The host galaxy of frb 20171020a revisited. *Publications of the Astronomical Society of Australia* 40:e029. https://doi.org/10.1017/pasa.2023.27.

Lorimer, D. R., M. Bailes, M. A. McLaughlin, D. J. Narkevic, and F. Crawford. 2007. A bright millisecond radio burst of extragalactic origin. *Science* 318 (5851): 777–780. ISSN: 00368075. https://doi.org/10.1126/science.1147532. arXiv: 0709.4301.

Macquart, J P, M B Bailes, N D R C Bhat, G C C Bower, J D D Bunton, S E Chatterjee, T A Colegate, et al. 2010. The commensal real-time askap fast-transients (craft) survey, 272–282.

Macquart, J. X. Prochaska, M. McQuinn, K. W. Bannister, S. Bhandari, C. K. Day, A. T. Deller, et al. 2020. A census of baryons in the universe from localized fast radio bursts. *Nature* 581, no. 7809 (May): 391–395. ISSN: 14764687. https://doi.org/10.1038/s41586-020-2300-2. arXiv: 2005.13161.

Maddox, N., B. S. Frank, A. A. Ponomareva, M. J. Jarvis, E. A.K. Adams, R. Davé, T. A. Oosterloo, et al. 2021. MIGHTEE-HI: The H » i emission project of the MeerKAT MIGHTEE survey. *Astronomy and Astrophysics* 646:1–14. ISSN: 14320746. https://doi.org/10.1051/0004-6361/202039655. arXiv: 2011.09470.

Mancera Piña, Pavel E., Justin I. Read, Stacy Kim, Antonino Marasco, José A. Benavides, Marcin Glowacki, Gabriele Pezzulli, and Claudia del P. Lagos. 2025. The galaxy-halo connection of disc galaxies over six orders of magnitude in stellar mass, arXiv: 2505.22727. http://arxiv.org/abs/2505.22727.

Mannings, Alexandra G., Wen-fai Fong, Sunil Simha, J. Xavier Prochaska, Marc Rafelski, Charles D. Kilpatrick, Nicolas Tejos, et al. 2021. A high-resolution view of fast radio burst host environments. *The Astrophysical Journal* 917 (2): 75. ISSN: 0004-637X. https://doi.org/10.3847/1538-4357/abff56.

Marchetti, Lucia, Thomas Jarrett, Angus Comrie, Alexander K. Sivitilli, Fabio Vitello, Ugo Becciani, and A. R. Taylor. 2022. iDaVIE-v: Immersive Data Visualisation Interactive Explorer for Volumetric Rendering. In *Astronomical data analysis software and systems xxx,* edited by Jose Enrique Ruiz, Francesco Pierfederici, and Peter Teuben, 532:85. Astronomical Society of the Pacific Conference Series. July. https://doi.org/10.48550/arXiv.2012.11553. arXiv: 2012.11553 [astro-ph.IM].

Matthews, L. D., W. van Driel, and J. S. Gallagher III. 1998. High-Resolution High Signal-to-Noise, Global H [CSC]i[/CSC] Spectra of Southern Extreme Late-Type Spiral Galaxies. *The Astronomical Journal* 116 (3): 1169–1185. ISSN: 00046256. https://doi.org/10.1086/300492.

McGaugh, Stacy S., and James M. Schombert. 2014. Color-mass-to-light-ratio relations for disk galaxies. *Astronomical Journal* 148 (5). ISSN: 00046256. https://doi.org/10.1088/0004-6256/148/5/77. arXiv: 1407.1839.

McMullin, J. P., B. Waters, D. Schiebel, W. Young, and K. Golap. 2007. CASA Architecture and Applications. In *Astronomical data analysis software and systems xvi,* 376:127. ASP Conference Series.

McQuinn, Matthew. 2014. Locating the "missing" baryons with extragalactic dispersion measure estimates. *Astrophysical Journal Letters* 780, no. 2 (January). ISSN: 20418205. https://doi.org/10.1088/2041-8205/780/2/L33. arXiv: 1309.4451.

Metzger, Brian D., Edo Berger, and Ben Margalit. 2017. Millisecond magnetar birth connects frb 121102 to superluminous supernovae and long-duration gamma-ray bursts. *The Astrophysical Journal* 841 (1): 14. ISSN 0004-637X. https://doi.org/10.3847/1538-4357/aa633d. arXiv 1701.02370. http://dx.doi.org/10.3847/1538-4357/aa633d.

Meyer, Martin, Aaron Robotham, Danail Obreschkow, Tobias Westmeier, Alan R. Duffy, and Lister Staveley-Smith. 2017. Tracing h i beyond the local universe. *Publications of the Astronomical Society of Australia* 34. ISSN 1323-3580. https://doi.org/10.1017/pasa.2017.31. arXiv: 1705.04210.

Michalowski, Michal J. 2021. Asymmetric h i 21 cm lines of fast radio burst hosts: connection with galaxy interaction. *The Astrophysical Journal Letters* 920 (1): L21. ISSN: 2041-8205. https://doi.org/10.3847/2041-8213/ac2b35.

Molnar, Daniel Cs, Mark T. Sargent, Sarah Leslie, Benjamin Magnelli, Eva Schinnerer, Giovanni Zamorani, and Jacinta Delhaize. 2021. The non-linear infrared-radio correlation of low-z galaxies: implications for redshift evolution, a new radio sfr recipe, and how to minimize selection bias. *Monthly Notices of the Royal Astronomical Society* 504 (1): 118–145. ISSN 13652966. https://doi.org/10.1093/mnras/stab746. arXiv: 2103.04803.

Nan, Rendong, D I Li, Chengjin Jin, Qiming Wang, Lichun Zhu, Wenbai Zhu, Haiyan Zhang, Youling Yue, and Lei Qian. 2011. *The five-hundred-meter aperture spherical radio telescope (fast) project.* Technical report. May https://doi.org/10.1142/S0218271811019335.

Perron-Cormier, Mathieu, Nathan Deg, Kristine Spekkens, Mark L. A. Richardson, Marcin Glowacki, Kyle A. Oman, Marc A. W. Verheijen, et al. 2025. *aj,* ISSN: 00046256. https://doi.org/10.3847/1538-3881/ada567 arXiv: 2501.09547. http://arxiv.org/abs/2501.09547%0Ahttp://dx.doi.org/10.3847/1538-3881/ada567.

Petroff, E., J. W.T. Hessels, and D. R. Lorimer. 2019. *Fast radio bursts,* 1 December. https://doi.org/10.1007/s00159-019-0116-6. arXiv 1904.07947.

Platts, E., A. Weltman, A. Walters, S. P. Tendulkar, J. E.B. Gordin, and S Kandhai. 2019. A living theory catalogue for fast radio bursts. *Physics Reports* 821:1–27. ISSN: 03701573. https://doi.org/10.1016/j.physrep 2019.06.003. arXiv: 1810.05836. https://doi.org/10.1016/j.physrep 2019.06.003.

Rajwade, K M, M C Bezuidenhout, M Caleb, L N Driessen, F Jankowski, M Malenta, V Morello, et al. 2022. First discoveries and localizations of fast radio bursts with meertrap : real-time , commensal meerkat sur v e y 1 i n t r o d u c t i o n 2 t h e m e e r t r a p s y s t e m *Monthly Notices of the Royal Astronomical Society* 1974:1961–1974. https://doi.org/10.1093/mnras/stac1450.

Ravi, Vikram and, Morgan Catha, Ge Chen, Liam Connor, Jakob T. Faber, James W. Lamb, Gregg Hallinan, et al. 2023. Deep synoptic array science: discovery of the host galaxy of frb 20220912a. *The Astrophysical Journal Letters* 949 (1): L3. ISSN: 2041-8205. https://doi.org/10.3847/2041-8213/acc4b6. http://dx.doi.org/10.3847/2041-8213/acc4b6.

Reynolds, T. N., T. Westmeier, and L. Staveley-Smith. 2020. H i deficiencies and asymmetries in hipass galaxies. *Monthly Notices of the Royal Astronomical Society* 499, no. 3 (December): 3233–3242. ISSN: 13652966. https://doi.org/10.1093/mnras/staa3126. arXiv: 2010.03720.

Reynolds, T. N., T. Westmeier, L. Staveley-Smith, G. Chauhan, and C. D.P. Lagos. 2020. H i asymmetries in lvhis, viva, and halogas galaxies. *Monthly Notices of the Royal Astronomical Society* 493 (4): 5089–5106. ISSN: 13652966. https://doi.org/10.1093/mnras/staa597. arXiv: 2002.11857.

Richter, O. -G., and R. Sancisi. 1994. Asymmetries in disk galaxies. How often? How strong? *Astronomy and Astrophysics* 290 (October): L9–L12.

Ryder, S D, K W Bannister, S Bhandari, A T Deller, R D Ekers, M Glowacki, A C Gordon, et al. 2023. *A luminous fast radio burst that probes the universe at redshift 1.* Technical report. https://www.science.org.

Saydjari, Andrew K., Edward F. Schlafly, Dustin Lang, Aaron M. Meisner, Gregory M. Green, Catherine Zucker, Ioana Zelko, et al. 2023. The Dark Energy Camera Plane Survey 2 (DECaPS2): More Sky, Less Bias, and Better Uncertainties. *The Astrophysical Journal Supplement Series* 264 (2): 28. ISSN: 0067-0049. https://doi.org/10.3847/1538-4365/aca594. arXiv: 2206.11909.

Shah, Vishwangi, Kaitlyn Shin, Calvin Leung, Wen-fai Fong, Tarraneh Eftekhari, Mandana Amiri, Bridget C. Andersen, et al. 2025. A repeating fast radio burst source in the outskirts of a quiescent galaxy. *The Astrophysical Journal Letters* 979 (2): L21. ISSN: 2041-8205. https://doi.org/10.3847/2041-8213/ad9ddc.

Shannon, R. M., K. W. Bannister, A. Bera, S. Bhandari, C. K. Day, A. T. Deller, T. Dial, et al. 2024. The commensal real-time askap fast transient incoherent-sum survey, no. Dm, ISSN: 14486083. https://doi.org/10.1017/pasa.2025.8. arXiv: 2408.02083. http://arxiv.org/abs/2408.02083.

Sharma, Kritti, Vikram Ravi, Liam Connor, Casey Law, Stella Koch Ocker, Myles Sherman, Nikita Kosogorov, et al. 2024. Preferential occurrence of fast radio bursts in massive star-forming galaxies. *Nature* (September). ISSN: 14764687. https://doi.org/10.1038/s41586-024-08074-9. http://arxiv.org/abs/2409.16964.

Shin, Kaitlyn, Calvin Leung, Sunil Simha, Bridget C. Andersen, Emmanuel Fonseca, Kenzie Nimmo, Mohit Bhardwaj, et al. 2024. Investigating the sightline of a highly scattered frb through a filamentary structure in the local universe, 1–20. arXiv: 2410.07307. http://arxiv.org/abs/2410.07307.

Skrutskie, M. F., R. M. Cutri, R. Stiening, M. D. Weinberg, S. Schneider, J. M. Carpenter, C. Beichman, et al. 2006. The Two Micron All Sky Survey (2MASS). *The Astronomical Journal* 131 (2): 1163–1183. ISSN: 0004-6256. https://doi.org/10.1086/498708.

Swarup, G., S. Ananthakrishnan, V. K. Kapahi, A. P. Rao, C. R. Subrahmanya, and V. K. Kulkarni. 1991. The Giant Metre-Wave Radio Telescope. *Current Science* 60 (January): 95.

van Cappellen, W. A., T. A. Oosterloo, M. A. W. Verheijen, E. A. K. Adams, B. Adebahr, R. Braun, K. M. Hess, et al. 2022. Apertif: Phased array feeds for the Westerbork Synthesis Radio Telescope. System overview and performance characteristics. 658 (February): A146. https://doi.org/10.1051/0004-6361/202141739. arXiv: 2109.14234 [astro-ph.IM].

van Eymeren, J., E. Jütte, C. J. Jog, Y. Stein, and R. -J. Dettmar. 2011. Lopsidedness in WHISP galaxies. II. Morphological lopsidedness. *Astronomy and Astrophysics* 530 (June): A30. https://doi.org/10.1051/0004-6361/201016178. arXiv: 1103.4929 [astro-ph.CO].

Wang, Jing, Bärbel S. Koribalski, Paolo Serra, Thijs van der Hulst, Sambit Roychowdhury, Peter Kamphuis, and Jayaram N. Chengalur. 2016. New lessons from the H I size-mass relation of galaxies. *Monthly Notices of the Royal Astronomical Society* 460 (2): 2143–2151. ISSN: 13652966. https://doi.org/10.1093/mnras/stw1099. arXiv: 1605.01489.

https://doi.org/10.1017/pasa.2025.10123 Published online by Cambridge University Press

Watts, Adam B., Barbara Catinella, Luca Cortese, and Chris Power. 2020. Xgass: robust quantification of asymmetries in global hi spectra and their relationship to environmental processes. *Monthly Notices of the Royal Astronomical Society* 3684 (3): 3672–3684. ISSN: 13652966. https://doi.org/10.1093/mnras/staa094. arXiv: 2001.04037.

Westmeier, T, S Kitaeff, D Pallot, P Serra, J M Van Der Hulst, R J Jurek, A Elagali, et al. 2021. Sofia 2 – an automated , parallel h i source finding pipeline for the wallaby survey. 16 (July): 1–16. arXiv: arXiv:2106.15789v1.

Westmeier, T., N. Deg, K. Spekkens, T. N. Reynolds, A. X. Shen, S. Gaudet, S. Goliath, et al. 2022. Wallaby pilot survey: public release of h i data for almost 600 galaxies from phase 1 of askap pilot observations. *Publications of the Astronomical Society of Australia* 39:1–23. ISSN: 14486083. https://doi.org/10.1017/pasa.2022.50. arXiv: 2211.07094.

Xu, Chen, Jie Wang, Yingjie Jing, Fujia Li, Hengqian Gan, Ziming Liu, Tiantian Liang, et al. 2024. Hifast: an hi data calibration and imaging pipeline for fast iii. standing wave removal, arXiv: 2411.13016. http://arxiv.org/abs/2411.13016.

Yu, Niankun, Luis C. Ho, and Jing Wang. 2020. On the determination of rotation velocity and dynamical mass of galaxies based on integrated h i spectra. *The Astrophysical Journal* 898 (2): 102. ISSN: 0004-637X. https://doi.org/10.3847/1538-4357/ab9ac5.

Yu, Niankun, Luis C. Ho, Jing Wang, and Hangyuan Li. 2022. Statistical analysis of h i profile asymmetry and shape for nearby galaxies. *The Astrophysical Journal Supplement Series* 261 (2): 21. ISSN: 0067-0049. https://doi.org/10.3847/1538-4365/ac626b. arXiv: 2203.13404. http://dx.doi.org/10.3847/1538-4365/ac626b.

https://doi.org/10.1017/pasa.2025.10123 Published online by Cambridge University Press

Appendix A: Additional Information

Table 5. Extra information for Figs. 1 and 2. Columns 3 and 4 display the resolution and RMS sensitivity of the bold (i.e. binned) spectra in each case in Fig. 1. Columns 5 and 6 display the HI column / surface densities as presented in Fig. 2, starting with the 3σ level as returned by SoFiA-2, and increasing by the multiples given in column 7.

FRB Name	Observation	Spectra		Moment Maps		
		Resolution (km s^{-1})	RMS (mJy)	3σ N_{HI} ($\times 10^{20}$ cm^{-2})	3σ Σ_{Hi} ($M_\odot$ pc^{-2})	Multiples
FRB 20181220A	GMRT	29.2	0.62	1.99	1.60	1,2,4,8
	FAST	12.9	0.30	-	-	-
FRB 20181223C	GMRT	11.6	1.32	1.36	1.09	1,2,4
	FAST	9.7	0.14	-	-	-
FRB 20190418A	GMRT	46.7	0.46	3.95	3.17	1,2,3,4
FRB 20190425A	GMRT	14.5	2.34	1.12	0.90	1,2,4,8
	FAST	12.9	0.99	-	-	-
FRB 20200223B	GMRT	10.4	0.50	-	-	-
	FAST	12.9	0.36	-	-	-
FRB 20200723B	MeerKAT	44.1	3.26	1.26	1.01	1,2,4,8
FRB 20201123A	MeerKAT	132.3	0.14	2.13	1.71	1,2,4
FRB 20210405I	MeerKAT	11.0	0.93	0.67	0.53	1,2,4,8
FRB 20211127I	MeerKAT	11.0	0.81	0.93	0.74	1,2,4,8,16
FRB 20211212A	MeerKAT	22.0	0.35	0.28	0.23	1,2,3
FRB 20231229A	MeerKAT	21.3	1.65	0.27	0.22	1,2,4
FRB 20231230A	MeerKAT	44.1	1.42	0.31	0.25	1,1.3,1.6,1.9
FRB 20240201A	MeerKAT	22.0	0.35	1.24	0.99	1,2,4,8,16
	FAST	12.9	0.20	-	-	-
FRB 20240210A	MeerKAT	11.0	0.95	2.39	1.91	1,2,4,8
FRB 20240312D	MeerKAT	22.0	0.34	1.20	0.96	1,2,4,8
FRB 20240615B	MeerKAT	11.0	0.43	0.27	0.22	1,2,4
FRB 20240615B	MeerKAT	10.4	5.94	0.27	0.22	1,2,4

https://doi.org/10.1017/pasa.2025.10123 Published online by Cambridge University Press

Appendix B: Asymmetry Metrics vs. Resolution

As outlined in Section 4.1, measuring the asymmetry metrics at various resolutions is particularly important for lower SNR targets. Fig. 11 demonstrates our methods for determining the optimal resolution at which to take measurements. Here we take a high resolution, lower SNR target (the host of FRB 20210405I), and display the values of A_{flux}, A_{spec}, and $A_{1\text{D}}$ as a function of rebinning factor. The values appear to be particularly unstable at low rebinning factors (due to noise) and high rebinning factors (due to resolution); these regimes are shown in red. The green region appears the most stable in all three metrics, with the central rebinning factor of 4 thus chosen as the one we use in our final asymmetry measurement.

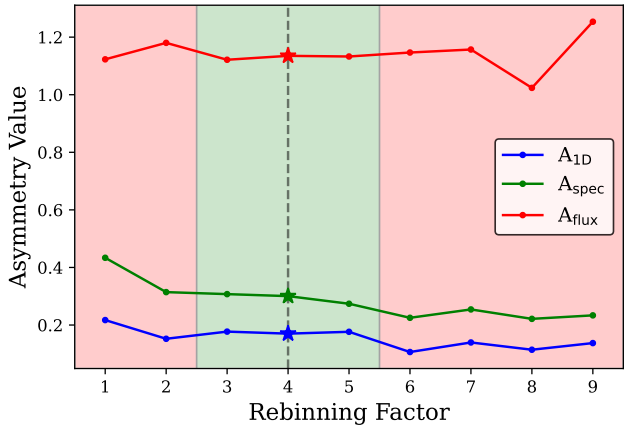

Figure 11. 1D asymmetry metrics for FRB 20210405I at various resolutions.

https://doi.org/10.1017/pasa.2025.10123 Published online by Cambridge University Press

Appendix C: Kinematic Modelling of FRB 20200723B

1603 –

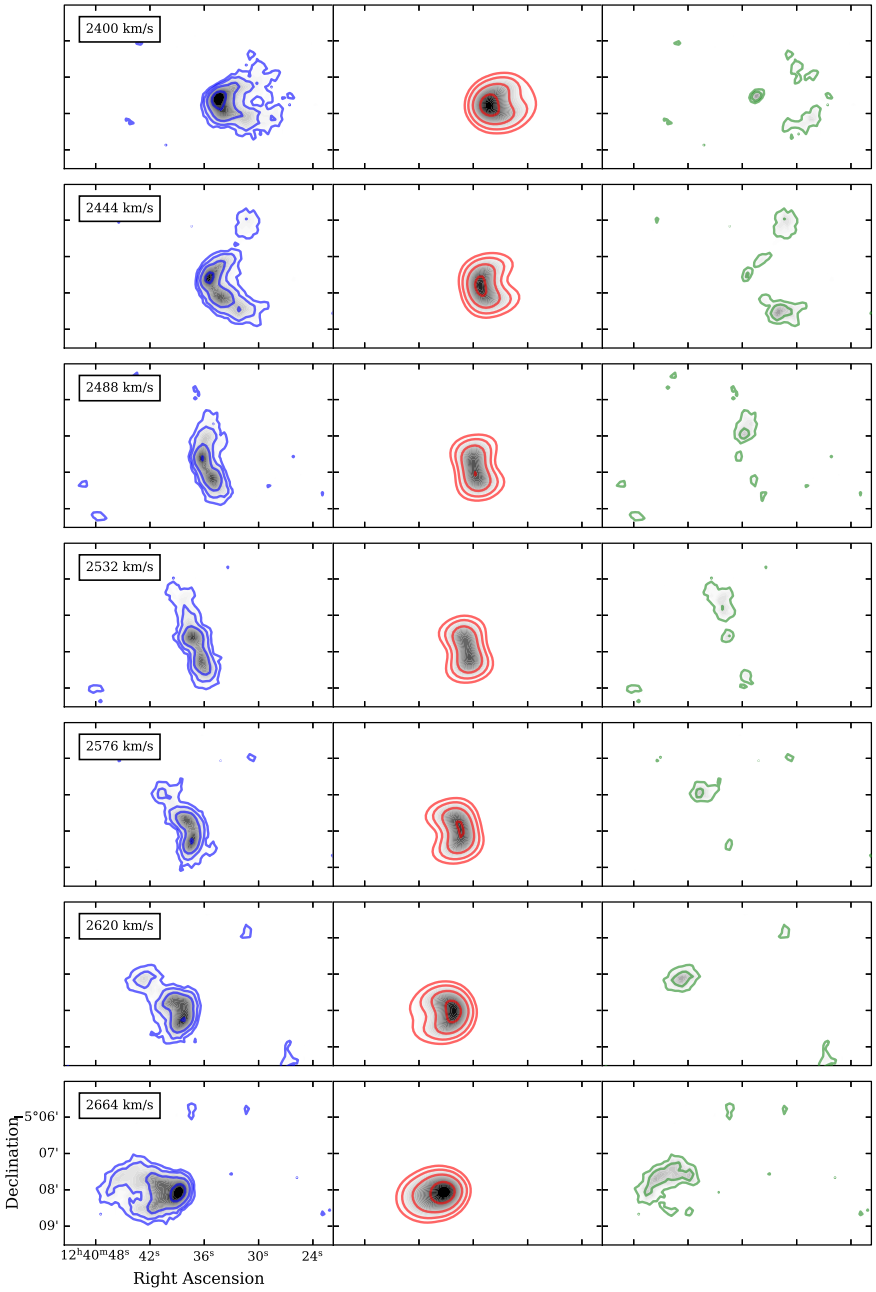

Figure 12. Comparison between observations of the host of FRB 20200723B (left) and a smooth rotating disk model from `3DBarolo` (centre), with residuals shown (right).

https://doi.org/10.1017/pasa.2025.10123 Published online by Cambridge University Press

Appendix D: Host Disturbance vs. HI Properties

Fig. 13 presents an identical plot to Fig. 8, just with FRB hosts colour-coded by our disturbance classification. Red targets are those we consider disturbed, orange are potentially disturbed, and green are settled.

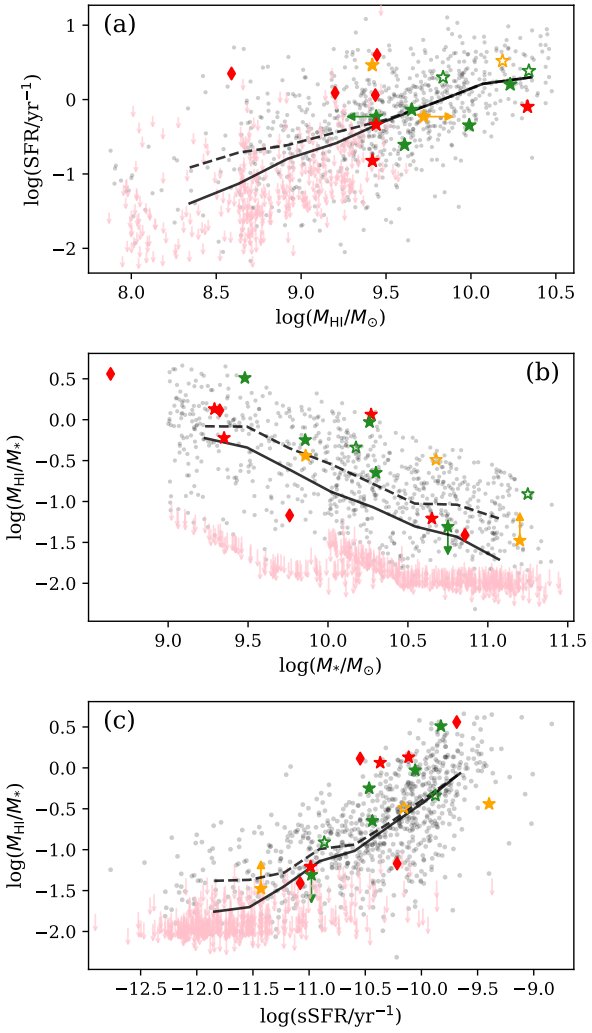

Figure 13. Same as Fig. 8 but with targets coloured by disturbance classification.

https://doi.org/10.1017/pasa.2025.10123 Published online by Cambridge University Press